VISCOSITY AND CRITICAL PROPERTIES OF N-DECANE, N-PENTADECANE AND N-EICOSANE USING MOLECULAR SIMULATION

by

Ibrar Ul Samad

A Thesis Presented to the Faculty of the
American University of Sharjah
College of Engineering
in Partial Fulfillment
of the Requirements
for the Degree of

Master of Science in
Chemical Engineering

Sharjah, United Arab Emirates

December 2019

Approval Signatures

We, the undersigned, approve the Master's Thesis of Ibrar Ul Samad.

Thesis Title: Viscosity and Critical Properties of n-Decane, n-Pentadecane and n-Eicosane using Molecular Simulation.

Signature **Date of Signature** (dd/mm/yyyy)

_____ _____

Dr. Naif Darwish
Professor, Department of Chemical Engineering
Thesis Advisor

_____ _____

Dr. Rachid Chebbi
Professor, Department of Chemical Engineering
Thesis Committee Member

_____ _____

Dr. Mohamed Al Zarooni
Associate Professor, Department of Chemical Engineering
American University of Ras Al Khaimah
Thesis Committee Member

_____ _____

Dr. Sameer Al-Asheh
Interim Head, Department of Chemical Engineering

_____ _____

Dr. Lotfi Romdhane
Associate Dean for Graduate Affairs and Research
College of Engineering

_____ _____

Dr. Naif Darwish
Acting Dean, College of Engineering

_____ _____

Dr. Mohamed El-Tarhuni
Vice Provost for Graduate Studies

Acknowledgements

In the Name of Allah, Most Kind, Most Merciful. All praises and thanks be to Allah and may His peace and blessings be upon Prophet Muhammad (PBUH), his family and his companions.

Firstly, I would like to profoundly offer my sincere gratitude and thanks to my advisor, Dr. Naif Darwish, for his continuous support, advice and guidance, especially in the early stages of the thesis selection process. Despite being burdened with administrative duties, he never hesitated or declined to meet up to discuss and offer his feedback about the thesis at different stages. I consider myself extremely lucky and privileged to have worked under the supervision of Dr. Naif, and simply thanking him would not be enough.

I would also like to offer my thanks and appreciation to my friend Mr. Muhammad Qasim, for providing valuable feedback and suggestions on the final thesis report. I would also like to thank him for the encouragement and advice on matters that are not only important for academics, but also for life. In addition, it would be my pleasure to offer thanks to my colleague and friend Engineer Abdollah Karami for helping me with the layout of the thesis report.

I am also grateful to Mr. Sarmad Saleem and Ms. Reem Jurri for their time and assistance to install the software necessary to carry out the research for the thesis.

I am also indebted to the Department of Chemical Engineering at the American University of Sharjah for providing me with the Graduate Teaching Assistantship that helped me develop my technical and interpersonal skills.

Special thanks go to the thesis committee members, Dr. Rachid Chebbi and Dr. Mohamed Al Zarooni, for providing useful remarks and suggestions at the early and final stages of the thesis that helped to make it better.

Lastly, my deepest and heartfelt gratitude goes to my parents for being my motivation and providing me with a reason to keep moving forward. Without their prayers, patience and constant love and support, I would have not reached where I am today.

Dedication

To my parents

Abstract

Studies involving heavy hydrocarbons have been steadily increasing due to the increase in the extraction of shale or heavy oil of which heavy hydrocarbons are a major constituent. Experimental studies are difficult to conduct on species found in heavy oil because of thermal instability that results in their decomposition at high temperatures. This is especially true in the case of determining critical properties. Additionally, extraction of pure species from heavy oil is difficult due to the high energy requirements. Since they are extrapolative in nature, existing correlations can be used but with a certain degree of inaccuracy. This study uses molecular simulation, mainly molecular dynamics, to predict viscosity, saturated liquid and vapor densities, and critical properties of three pure heavy n-alkanes, namely, n-decane, n-pentadecane and n-eicosane. The viscosity was predicted as a function of temperature using equilibrium molecular dynamics with the Green-Kubo relations and the AMBER force-field. Comparison with experimental data showed that the AMBER force-field predicts reasonably the viscosity of smaller molecules at higher temperatures. The percentage deviation for n-decane was 40% at 300 K and 25% at 500 K. On the other hand, for n-pentadecane and n-eicosane, the percentage deviations were 34.7% at 550K and 76.2% at 600 K, respectively. For the critical properties, which were determined from the simulated saturated liquid and vapor densities, AMBER, COMPASS and TraPPE force fields were employed. For all three force fields, the methodology of volume-expansion molecular dynamics was used, while the Gibbs ensemble Monte Carlo technique was used with the AMBER force field. The results were compared with experimental data, as well as with those from several correlations and equations-of-state. The results show that the TraPPE force field is the most accurate in predicting critical properties (less than 10% deviation), followed by AMBER (less than 20% deviation, except for the critical pressures for n-eicosane) and COMPASS (up to 24% deviation). Finally, a comparison was made for the needed computational time; COMPASS required the largest execution time, followed by AMBER and TraPPE.

Search Terms: Molecular Dynamics, Monte Carlo, Heavy Hydrocarbons, Viscosity, Critical Properties

Table of Contents

List of Figures

List of Tables

Chapter 1. Introduction

1.1 Overview

Due to the continuous increase in world energy demand and the rapid depletion of conventional petroleum resources, emphasis is being placed on increased extraction and utilization of unconventional oil resources in the form of shale or heavy oil [1], [2]. These heavy oil resources are much larger than conventional oil resources, which has contributed to their increased production in the oil and gas industry. In China alone, for example, it has been estimated that the resources of heavy oil reach about 6×10^9 tons [3], which are less than those of Canada [4] and Venezuela, where both countries are estimated to have 2 – 3 trillion barrels of unconventional oil resources, each [5]. Figure 1 below displays the production history of heavy oil in Canada, which leads the world in terms of production of heavy oil.

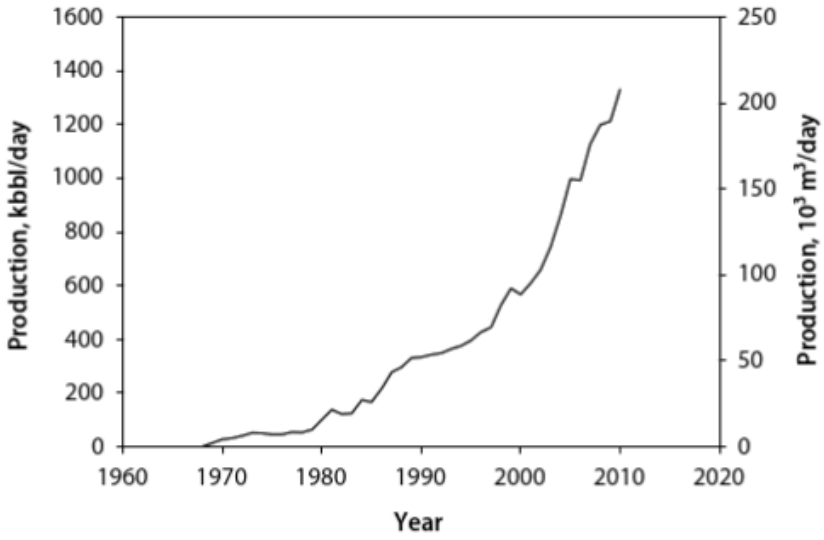

Figure 1: Heavy Oil production history in Canada [4].

It is evident from Figure 1 that the trend of heavy oil production will continue to increase in the future. Hence, it is anticipated that petroleum resources, and specifically unconventional oil, will be important sources of energy for the world in the future [6].

However, the oil extracted from these reserves is heavy and highly viscous. As per the definitions provided by the American Petroleum Institute (API), any liquid petroleum having an API gravity less than 22° is defined to be heavy oil. Whereas, an

API gravity of less than 10° is considered to be "extra-heavy" oil [1], [2], [7]. Furthermore, heavy oil also has a viscosity in the range of 10^2-10^4 cP [1], [8], [9]. The highly viscous nature of the heavy oil is due to the presence of a higher percentage of asphaltenes, aromatics, resins and saturated hydrocarbons that are generally made up of over 15 carbon atoms [2], [8]. Additionally, the concentrations of heavy metals, sulfur and nitrogen are found to be higher in heavy oil than in conventional oil [9]. Table 1 below, presents the ranges of typical weight percentage (composition) for heavy and conventional oil:

Table 1: Compositional comparison between conventional and heavy oil [2].

Sample	**Typical composition range (wt. %)**		
	Asphaltenes	**Resin**	**Saturates & Aromatics**
Conventional oil	<0.1-12	3-22	67-97
Heavy oil	11-45	14-39	24-64

Because of the increase in the production of the heavy oil; it is imperative to study the different thermophysical properties associated with the individual constituents of the heavy oil. Determination of the critical properties and viscosity of the heavy hydrocarbons that make up the heavy oil is not an easy task. This is so because heavy hydrocarbons are prone to thermal degradation at higher temperatures, i.e., they become thermally instable. Lack of available thermophysical data on heavy hydrocarbons has led to a slow development of heavy oil production [10]. The critical properties of heavy hydrocabons are essential to predict various thermodynamic and volumetric properties, in order to design processes for both production and refining of crude oils [11]. For example, cubic equation of states (EOS), such as Soave-Redlich-Kwong and Peng-Robinson, are used in the petroleum industry to perform phase equilibrium calculations. However, in order to perform such calculations using the EOS, it is essential to precisely know the critical properties of the hydrocarbon species [12]. Although experimentation is the best method to determine the critical properties of pure components and mixtures; heavy hydrocarbons thermally decompose before the critical point is achieved, thereby making experimentation not an option for

determining the critical properties [11]–[13]. Moreover, the knowledge of the viscous nature of heavy oil allows the design of processes that would make heavy oil pipeline transportable [8]. Therefore, analytical methods are required to predict the critical properties and viscosities of the heavy hydrocarbons that are present in heavy oil.

One method that can be used for the prediction of the critical properties of heavy hydrocarbons is applying correlations. Estimation of thermophysical properties using correlations usually incurs a certain degree of inaccuracy, due to their inefficient extrapolative power. New techniques are, therefore, required to predict the thermophysical properties of heavy hydrocarbons, such as critical temperature, since experimental determination of these properties is extremely difficult and very costly [11].

An important technique that can predict the critical and other thermophysical properties, such as viscosity, is based on molecular simulations and modelling. Molecular simulations are now increasingly being used to predict the thermophysical properties of pure species and mixtures over a range of temperatures and pressures [14]. Here, thermophysical properties of macroscopic systems are predicted by following the interactions among a limited number of system constituents (molecules, atoms, or ions) in a certain special region under fixed (known a priori) external set of constraints (ensembles). Such interactions in a simulation can be primarily studied either using the Monte-Carlo (MC) method (a stochastic method) or the molecular dynamics (MD) method (a deterministic method). The results from these simulations are used to complement experimental data and also provide an insight into a system at molecular level [14].

1.2 Thesis Objectives

The aim of this work is to employ molecular simulation, MC and MD, to predict selected thermophysical properties (critical and viscous properties) of pure heavy chemical species belonging to specific family of n-alkanes. The species studied are n-decane (C10) as a reference compound, n-pentadecane (C15) and n-eicosane (C20). Specifically, the following tasks will be carried out:

1. Prediction of the critical properties of the selected heavy n-paraffins using MD (with three different force-fields) and MC

2. Prediction of the viscosities using the Green-Kubo MD simulations
3. Comparison of the predicted critical properties using different force-fields in the case of MD
4. Comparison of the computational time for different force-fields

1.3 Thesis Organization

This thesis is organized as follows:

- Chapter 1 provides with an introduction to the problem at hand and objectives that are to be carried out in the thesis.
- Chapter 2 deals with the literature review on molecular simulations (including statistical mechanics theory) and the different techniques and methods used to predict viscosities and critical properties.
- Chapter 3 gives the methodology used to carry out the simulations and also provides details on the software used, along with the parameters for the different force-fields employed.
- Chapter 4 provides the results generated for viscosity, critical properties and the computational efficiency.
- Chapter 5 provides conclusions and recommendations based on the simulation work carried out in this thesis.

Chapter 2. Literature Review

2.1 Ensembles and Statistical Mechanics

The fundamental framework for carrying out molecular simulations is provided by statistical mechanics [14], [15]. The aim of statistical mechanics is to provide the theoretical basis that would define the macroscopic properties (such as temperature, pressure, volume, energy, etc.) of the state of a system (i.e. the macrostate) from the microscopic description of the same system. The microscopic description of the state of a system is completely specified by the velocities and positions of all system constituents, which in turn specify the energy level of the system for that state. Such a state is known as the quantum state or microstate. Hence, for any given macrostate, there exists many different quantum states [14], [16]–[20]. Figure 2 below summarizes the concept of macrostates and quantum states:

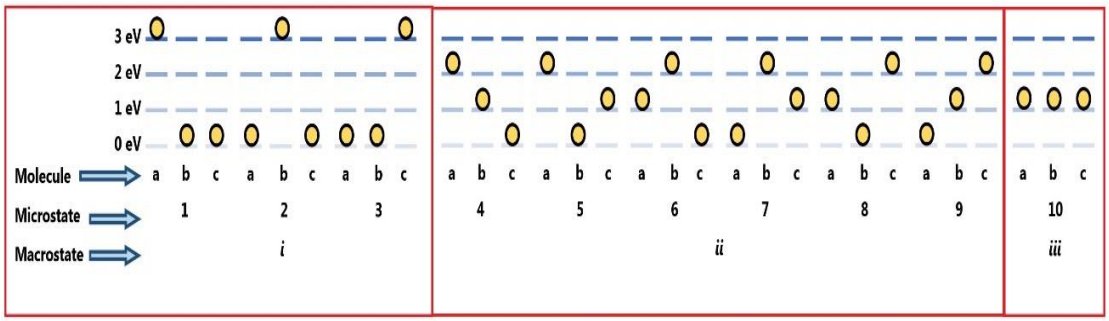

Figure 2: Depiction of macrostates and microstates. The macrostate in this example must have a total energy of 3 eV.

In Figure 2, the macrostate is defined to have a total energy of 3eV. In order to satisfy this condition, ten different quantum states exist. For example, in macrostate *i*, only one particle is required to be at the third energy level. This particle could be any of the three particles (a, b, or c); but a different particle would correspond to a different quantum state in the same macrostate. Therefore, a given macrostate corresponds to many different possible microstates.

In order to perform a priori calculation of a given thermodynamic property, such as pressure, from the molecular description of a system, quantum and/or classical mechanics would need to be used to calculate the force per unit area exerted on the walls of such a system. Additionally, such exerted force would fluctuate with time, hence, a sufficiently long period of time would be required in order to smooth out the

fluctuations. However, because of the large number of particles involved (of the order of ~ 10^{23}) and the large number of quantum states available for a given macrostate, carrying out such calculations would be a near impossible task, even with the use of supercomputers computers [19]–[21].

The solution to this problem was proposed by Gibbs employing the concept of ensembles. The ensemble is a mental or virtual collection of a large number of systems, Π. Each of these systems in the ensemble is a replica of the macroscopic system that is being studied. For example, given a macroscopic system that has N number of molecules of a total volume V and a temperature T, the ensemble would have Π systems that would replicate the N, V and T of the macroscopic system. The Π systems are all identical on a macroscopic level, however, on the microscopic level each system in the ensemble would correspond to a certain quantum state. Therefore, at any instant of time, many quantum states would be represented by the various systems in the ensemble [16]–[21]. Continuing with the example of calculating pressure, each of the quantum states would then give a different instantaneous pressure. By giving equal weightage to each system in the ensemble, the "ensemble average" can be calculated by using the average of the instantaneous pressures in each quantum state [20]. Furthermore, after equilibrium has been established, the differences in the instantaneous pressure are very small, and hence, negligible [19]. This leads to the main conclusion of Gibbs idea, known as the "ergodic postulate", which states:

> The time average of any thermodynamic variable φ in an actual system is equal to the ensemble average of φ in the limit as the number of replicas Π in the ensemble goes to infinity, provided that the members of the ensemble copy precisely the thermodynamics state and environment of the actual system, that is, adhere to the specified macroscopic conditions. [19]

Equation (1) below summarizes ergodic postulate for a thermodynamic property, A:

$$A_{macro} = \langle A \rangle_{time} = \langle A \rangle_{ensemble} \quad (1)$$

In Equation (1), the subscripts *macro*, *time*, and *ensemble*, respectively represent the thermodynamic property in macroscopic conditions, time average of an actual system, and ensemble average.

In molecular simulations, statistical ensembles are used to conceive many microstates that would result in the conditions that are desired in the macrostate. In general, the ensemble is subject to the same constraints imposed of the studied macroscopic system. As such, it is usually constrained by a set of three properties that represent the external constraints on the macroscopic system, such as fixed *N*, *V*, and *T* or fixed *N*, *E*, and *V*. These constraints are usually selected based on the properties that need to be studied in the macroscopic system and are similar to those of an experimental set-up. Therefore, different ensembles are used throughout molecular simulations [14]–[16], [19], [21]. The properties that are not constrained will fluctuate throughout the simulation and can be predicted by analyzing the simulation results using the formulation of statistical mechanics [14].

As stated previously, molecular simulations are usually carried out by two main methods, MD and MC. MD, a deterministic method, follows the time evolution of a system by numerically integrating Newton's equations of motion [14]–[16], [19], [21], [22]. Equation (2) below presents the statistical average for a thermodynamic property *A* [14], [22] using the MD approach:

$$\langle A \rangle_{macro} = \langle A \rangle_{time} = \lim_{t \to \infty} \frac{1}{t} \int_0^t A(t) dt \approx \left(\frac{1}{M_t} \right) \sum_{i=1}^{M_t} A_i(t) \tag{2}$$

where t is the simulation time and M_t is the number of time steps conducted in the simulation.

MC, in contrast to MD, is based on the probability of finding a macroscopic system in a certain quantum state and is thus a stochastic method. Successive configurations of a system are generated using statistics that respect the probability distribution of the system [22]. In order to calculate the statistical average for a property; Equation (3) is used [14]:

$$\langle A \rangle_{macro} = \langle A \rangle_{ensemble} = \int_{PS} A(PS) \left(\frac{e^{-\beta E(PS)}}{Z} \right) d(PS) \approx \sum^{N_{micro}} A(PS) \left(\frac{e^{-\beta E(PS)}}{Z} \right) d(PS) \tag{3}$$

where *PS* is the phase space of possible configurations, i.e. tracking the position and momentum of *N* particles in a 6N dimensional space. While *Z* is the partition function

that enables the calculation of thermodynamic properties, E is the total energy and β is the thermodynamic beta. Equation (4) below, presents the thermodynamic beta (with k_B being the Boltzmann constant) [22]:

$$\beta = \frac{1}{k_B T} \tag{4}$$

As can be seen from Eqns. (1), (2) and (3), both MD and MC provide the same results for a system that is at equilibrium. The relationship between MD and MC is illustrated in Figure 3 below:

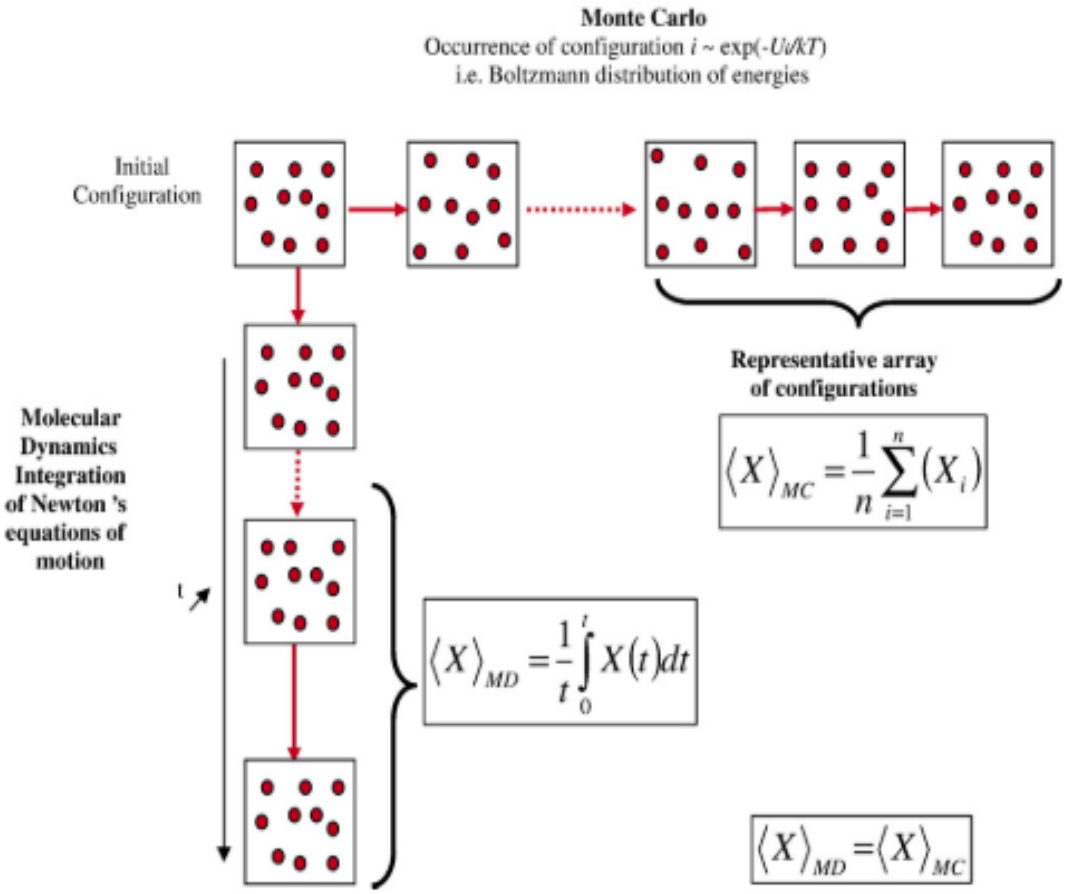

Figure 3: Monte-Carlo and Molecular dynamics concept [22].

2.1.1 Microcanonical (NVE) ensemble. The microcanonical ensemble describes an isolated system with fixed N, V and E (total energy). This represents a system with impermeable, rigid and adiabatic walls. Figure 4, represents the microcanonical ensemble:

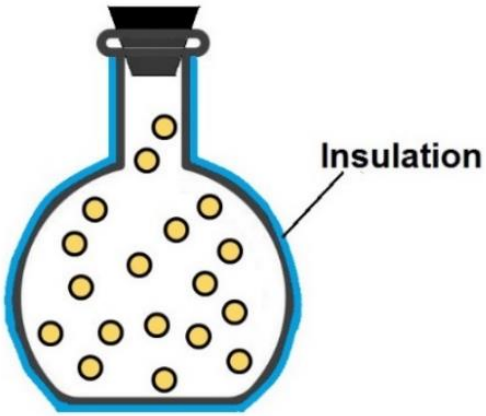

Figure 4: The microcanonical ensemble (const. *N*, *V* and *E*).

Although the constraint of having fixed energy will correspond to a certain temperature; the microcanonical ensemble is rarely used in molecular simulations because of the difficulty in replicating experimental set-up [14]. Hence, it is mostly used for carrying out fundamental theoretical concepts [18]. However, it has been reported to provide various transport and vibrational properties of liquid water [23], as well as the diffusion of water through carbon nanotubes [24]. Additionally, the microcanonical ensemble has also recently been used to study the dispersion curves of water [25] and viscosities of branched alkanes for a range of pressures [26] in combination with other ensembles. Lastly, the oxidation of aluminum nanoparticles in the presence of oxygen has also been simulated using the microcanonical ensemble [27].

In the microcanonical ensemble, it is reasonable to postulate that all microstates have an equal probability of being accessible (equal a priori probability [18]) as long as they satisfy the macroscopic conditions [16], [18], [28]. The thermodynamic probability (Ω_j, possible number of microstates in a given configuration, *j*) in a system of distinguishable particles can be calculated using Equation (5) [14]:

$$\Omega_j = \frac{N!}{\prod_{i=1} N_i!} \tag{5}$$

where N_i is the distribution of particles on different energy levels in a quantum state. For the example shown in Figure 1, calculating the number of microstates for the first configuration where only one particle is required to be at the third energy level is as shown in Equation (6):

$$\Omega_1 = \frac{3!}{1!\,2!} = 3 \tag{6}$$

Additionally, the true probability, p_j, of the system can be calculated using the total thermodynamic probability, Ω, as shown in Equation (7) [19], [20]:

$$p_j = \frac{\Omega_j}{\Omega} \tag{7}$$

Furthermore, using the Gibbs entropy equation (Equation (8)) and the fact that the sum of the true probability equals 1; the famous Boltzmann entropy equation is derived (Equation (9)) [16], [17], [19], [20]:

$$S = -k_B \sum_{j=1} p_j \ln(p_j) \tag{8}$$

$$S = k_B \ln(\Omega) \tag{9}$$

The Boltzmann entropy equation is one of the most significant equations as it bridges the gap between classical and statistical thermodynamics. Several thermodynamics properties can be derived by using Equation (9) with the relationships present in classical thermodynamics [14], [16], [18], [20].

Lastly, the microcanonical partition function is provided in Equation (10) below [15]:

$$Z_{NVE} = \sum_{PS} \delta[\mathcal{H}(PS) - E] \tag{10}$$

where $\mathcal{H}$ is the Hamiltonian and δ is the Kronecker delta according to the conditions given below:

$$\delta = 1, if\ E < \mathcal{H}(PS)$$

$$\delta = 0, else.$$

2.1.2 Canonical (NVT) ensemble. In the canonical ensemble, the number of particles *N*, the temperature *T*, and the volume *V*, are held constant [22], [29]. This ensemble is the most commonly used ensemble in statistical thermodynamics [18]. Average properties predicted from this ensemble are the total energy, pressure and

chemical potential [22]. The partition function for the canonical ensemble is calculated as shown in Equation (11) [14], [18], while Figure 5 depicts the ensemble.

$$Z_{NVT} = \sum_{i} e^{-(\beta E_i)} \tag{11}$$

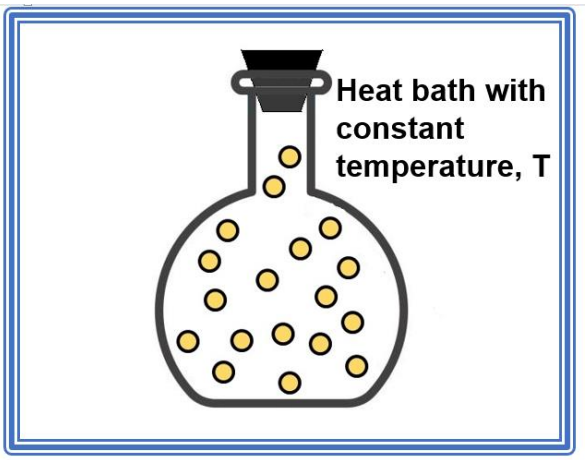

Figure 5: Canonical ensemble at fixed *N*, *V* and *T*

The canonical ensemble is mainly used to study phase properties, such as constant volume heat capacity, enthalpy, chemical potential, etc. [22], [30]–[32]. Furthermore, the canonical ensemble in MC simulations (known as the Gibbs ensemble) has been employed to calculate vapor liquid equilibria of pure species and mixtures and their critical properties [33]–[38].

2.1.3 Isothermal-isobaric (NPT) ensemble. This ensemble, as the name suggests, imposes a constant pressure *P*, temperature *T*, and a constant number of particles *N*, as depicted in Figure 6.

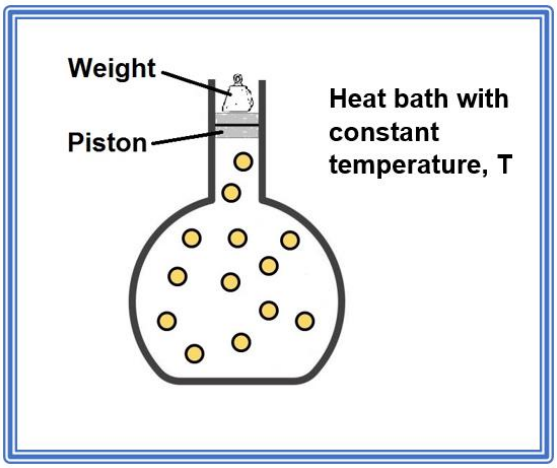

Figure 6: Isothermal-isobaric ensemble. Fixed *N*, *P* and *T*.

The NPT ensemble is one of the most widely used ensembles in molecular simulations, especially in MC simulations. This is because most real experiments are conducted at constant temperature and pressure. It is worth mentioning that this ensemble has been used in connection with virial expansion for pressure in order to verify the equation of state [29].

Equations (12) and (13) displays the partition function of this ensemble derived from the canonical ensemble respectively [14]–[16], [18]:

$$Z_{NPT} = \sum_{V_j} \sum_{i} e^{-(\beta E_i)} e^{-(PV_j * \beta)} \tag{12}$$

$$Z_{NPT} = \sum_{V_j} Z_{NVT} e^{-(PV_j * \beta)} \tag{13}$$

Similar to the canonical ensemble, the NPT ensemble is used to study the phase properties of different species and mixtures at a given temperature and pressure [22]. For example, MD simulations have been conducted to study the formation of ice at high pressures [39] and the cage occupancy of methane in methane hydrates [40]. MC simulations have also been conducted using the NPT ensemble to develop phase equilibria of systems such as dipropylene glycol, dipropylene ether and water [41] and methane & n-butane [42]. Moreover, the NPT ensemble can also be used to predict the equilibrium properties (such as molar volume, isothermal compressibility, speed of sound, etc.) of ionic liquids [43].

2.1.4 Grand Canonical (VTμ) ensemble. For some simulations, it is required to know the average number of particles based on the external conditions. For example, in adsorption studies it is desired to know the amount of a material adsorbed on the surface of the adsorbent as a function of temperature and pressure. In the Grand-Canonical ensemble, volume, temperature and the chemical potential μ_i are imposed, as depicted in Figure 7 [22], [29]. The probability density of this ensemble is given in Equation (14) [22]:

$$Z_{VT\mu} = \sum_{i} \sum_{j} e^{-(VE_j * \beta)} e^{(\mu N_i * \beta)} \tag{14}$$

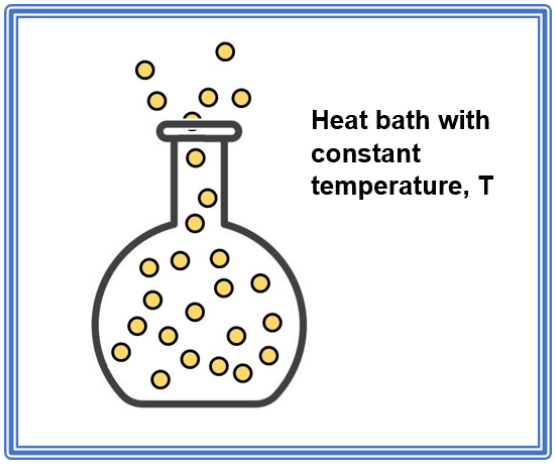

Figure 7: Grand canonical ensemble. *V*, *T* and μ are fixed.

The VTμ ensemble is again more adapted for use in MC simulations rather than the MD simulations, which, when used, is mainly employed for simple systems [29]. The VTμ ensemble is best suited for adsorption studies. However, in order to carry out the simulations, the interaction energies between the adsorbent and the adsorbate must be specified [22]. Several studies have been conducted that use the grand canonical ensemble to study the effects of adsorption, such as:

- Adsorption of dye N719 on titanium oxide [44]
- Adsorption of benzene and toluene on activated carbon [45]
- Study of pyridine adsorption on different adsorbents [46]
- Studies involving adsorption of natural gas [47], ethane and ethylene [48], and gases such as CO_2 and nitrogen [49] on metal organic frameworks

2.1.5 Partition function and thermodynamic properties. The partition function is a key concept in statistical thermodynamics and is used to calculate and derive properties from relationships available in classical thermodynamics. For a given ensemble, the partition function is essentially the sum of all available states. It is a fundamental property in statistical thermodynamics that is similar to the fundamental thermodynamic relations in classical thermodynamics, thus allowing the calculation of various thermodynamic properties [14].

The following sections provide a summary of different thermodynamic properties available for the ensembles discussed above, derived from fundamental thermodynamic relations. Equations (15)-(19) provide the thermodynamic properties

for the microcanonical (NVE) ensemble, while Equations (20)-(25) represent the thermodynamic properties for the canonical (NVT) ensemble. For the NPT ensemble, Equations (26)-(30) are used to calculate the different thermodynamic properties [14], [18]. Lastly, Equations (31)-(35) are used for the grand canonical (VTμ) ensemble [14], [18].

2.1.5.1 *Microcanonical (NVE) ensemble*

$$S = k_B \ln(\Omega) \tag{15}$$

$$dS = \frac{1}{T} dE + \frac{P}{T} dV - \frac{\mu}{T} dN \tag{16}$$

$$\frac{1}{T} = k_B \left(\frac{\partial(\ln(\Omega))}{\partial E} \right)_{N,\ V} \tag{17}$$

$$\frac{P}{T} = k_B \left(\frac{\partial(\ln(\Omega))}{\partial V} \right)_{N,\ E} \tag{18}$$

$$\frac{\mu}{T} = -k_B \left(\frac{\partial(\ln(\Omega))}{\partial N} \right)_{V,\ E} \tag{19}$$

2.1.5.2 *Canonical (NVT) ensemble*

$$S = k_B \ln(\mathrm{Z}_{NVT}) + k_B T \left(\frac{\partial \mathrm{Z}_{NVT}}{\partial T} \right)_{N,\ V} \tag{20}$$

$$A = -k_B T \ln(\mathrm{Z}_{NVT}) \tag{21}$$

$$dA = -SdT - PdV + \mu dN \tag{22}$$

$$\frac{P}{T} = k_B \left(\frac{\partial(\ln(\mathrm{Z}_{NVT}))}{\partial V} \right)_{N,\ T} \tag{23}$$

$$\frac{\mu}{T} = -k_B \left(\frac{\partial(\ln(\mathrm{Z}_{NVT}))}{\partial N} \right)_{V,\ T} \tag{24}$$

$$\frac{E}{T^2} = k_B \left(\frac{\partial(\ln(\mathrm{Z}_{NVT}))}{\partial E} \right)_{N,\ V} \tag{25}$$

2.1.5.3 *Isothermal-isobaric (NPT) ensemble*

$$S = k_B \ln(\mathrm{Z}_{NPT}) + k_B T \left(\frac{\partial \mathrm{Z}_{NPT}}{\partial T}\right)_{N,\ P} \tag{26}$$

$$G = -k_B T \ln(\mathrm{Z}_{NPT}) \tag{27}$$

$$dG = -SdT + VdP + \mu dN \tag{28}$$

$$\frac{V}{T} = -k_B \left(\frac{\partial(\ln(\mathrm{Z}_{NPT}))}{\partial P}\right)_{N,\ T} \tag{29}$$

$$\frac{\mu}{T} = -k_B \left(\frac{\partial(\ln(\mathrm{Z}_{NPT}))}{\partial N}\right)_{P,\ T} \tag{30}$$

2.1.5.4 *Grand canonical (VTμ) ensemble*

$$S = k_B \ln(\mathrm{Z}_{VT\mu}) + k_B T \left(\frac{\partial \mathrm{Z}_{VT\mu}}{\partial T}\right)_{N,\ \mu} \tag{31}$$

$$PV = k_B T \ln(\mathrm{Z}_{VT\mu}) \tag{32}$$

$$d(PV) = SdT + PdV + Nd\mu \tag{33}$$

$$\frac{N}{T} = k_B \left(\frac{\partial(\ln(\mathrm{Z}_{VT\mu}))}{\partial \mu}\right)_{V,\ T} \tag{34}$$

$$\frac{P}{T} = k_B \left(\frac{\partial(\ln(\mathrm{Z}_{VT\mu}))}{\partial V}\right)_{\mu,\ T} = \frac{k_B \ln(\mathrm{Z}_{VT\mu})}{V} \tag{35}$$

2.2 Inter-and-Intra Molecular Energy

The formulations derived in statistical thermodynamics are dependent on the total energy of the system, which is the sum of the kinetic and potential energy. Computation of the kinetic energy using MD is straightforward (Equation (36)) [50]. While in MC, the kinetic energy is calculated through analytical integration and therefore, does not need to be performed explicitly [22].

$$KE(t) = \frac{1}{2}\sum_{i=1}^{N} m_i (v_i(t))^2 \tag{36}$$

Therefore, it is the calculation of the potential energy that is required in order to accurately compute thermophysical properties, as it needs to be provided on the basis of the molecular coordinates of the system [22], [50]. Hence in molecular simulations, one key factor that affects the outcome of the results is the molecular interaction model used to calculate the potential energy among the different molecular species [14]. The total potential energy is usually decomposed into two main components as shown in Equation (37) below [22]:

$$E_{pot} = E_{int} + E_{ext} \tag{37}$$

where E_{int} is the intramolecular energy and E_{ext} is the external or intermolecular energy. The intermolecular energy term is fundamentally the energy due to the interactions between the system's constituents.

Equation (37) can be further expanded according to a modern molecular potential energy model, as displayed in Equation (38) [14], [21], [26], [51]. Generally, the first four terms represent the energy from the intramolecular interactions, while the last two are forms of the intermolecular interactions.

$$E_{pot} = \sum_{stretch} E_{AB} + \sum_{bend} E_{ABC} + \sum_{dihedral} E_{AB} + \sum_{out-of-plane} E_{ABCD} + \sum_{non-bonded} E_{ABCD} + \sum_{Coulomb} E_{AB} \tag{38}$$

2.2.1 Bond stretching. Assuming Hooke's law is applicable, the stretching of the bonds between atoms A and B will contribute to the total molecular potential energy of the system. The energy from this source is calculated using Equation (39) [14], [21], [33], [51], [52].

$$E_{AB} = \frac{1}{2} k_{AB} \left(R_{AB} - R_{e,AB} \right)^2 \tag{39}$$

where k_{AB} is the force or spring constant, R_{AB} is the instantaneous bond length and $R_{e,AB}$ is the equilibrium bond length. Figure 8 depicts the stretching of a bond for a butane molecule.

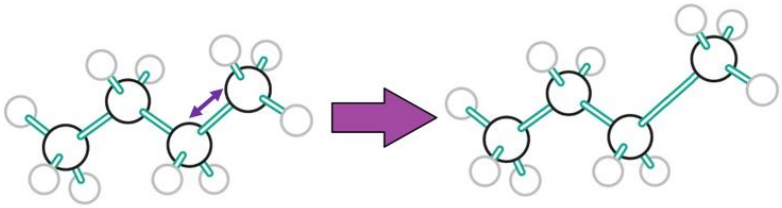

Figure 8: Stretching of a bond.

2.2.2 Bond bending. It is normal to consider the energy due to the bending vibrations between three connected atoms A-B-C as provided by Equation (40) [14], [21], [33], [51], [52]:

$$E_{ABC} = \frac{1}{2} k_{ABC} \left(\theta_{ABC} - \theta_{e,AB} \right)^2 \tag{40}$$

where k_{ABC} is the spring constant and θ is the angle between the atoms. The symbol e again represents the equilibrium value. For a butane molecule; Figure 9 presents an example of bond bending:

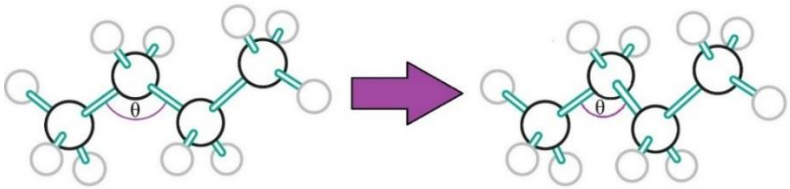

Figure 9: Bond bending.

2.2.3 Dihedral motions (Torsion). Considering four atoms linked together, ABCD, there might be either full rotation (known as proper dihedral, see Figure 10) or partial rotation (improper dihedral) about the backbone of the molecule, B-C.

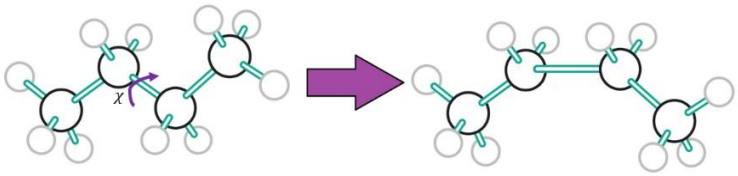

Figure 10: Dihedral angle, χ, for a butane molecule.

The energy associated can be calculated using Equation (41) as follows [14], [21], [33], [51]:

$$E = \frac{U_o}{2} \left(1 - cos\left(n(\chi - \chi_e) \right) \right) \tag{41}$$

where n is the periodicity parameter; for example, a methyl group would have the periodicity parameter as 3. χ is the torsion angle and U_o is the torsional rotation force constant.

2.2.4 Out-of-plane angle potential (inversion). For a molecule of four atoms, such as ammonia, changing the inversion angle (ψ) from positive to negative inverts the molecule (see Figure 11).

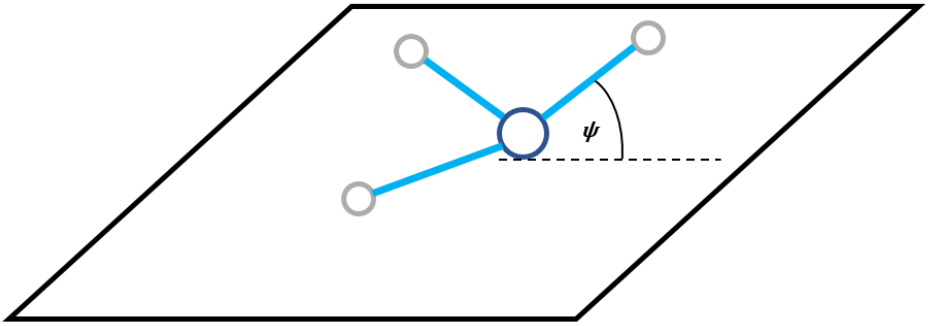

Figure 11: Inversion potential.

The potential energy from this contribution can be calculated using Equation (42) [14], [21], [33], [51]:

$$E = k_1(1 + cos(n\psi - k_2)) \tag{42}$$

Again, n represents the periodicity parameter, k_1 and k_2 are constants set at the beginning of the experiment and ψ is the angle of inversion.

2.2.5 Non-Bonded interactions. Key non-bonded interactions are dispersion-repulsion energy between atoms of different molecules [22] or of atoms within the same molecule at a distance of 3 bonds or more [36]; thus requiring the calculation of intermolecular energy. Many potentials are available for calculating the dispersion-repulsion energy such as Born-Mayer-Huggins potential (used when dealing with polar species), Buckingham exp-6 model, and the most extensively used and popular model, that is the Lennard-Jones (LJ) 6–12 model. Equation (43) below, present the LJ 6-12 model [14]–[16], [18], [19], [21] :

$$E_{LJ} = 4\varepsilon_{ij}\left(\left(\frac{\sigma_{ij}}{r_{ij}}\right)^{12} - \left(\frac{\sigma_{ij}}{r_{ij}}\right)^{6}\right) \tag{43}$$

where r_{ij} is the separation distance between force centers of particles i and j, ε_{ij} is the energy at minimum E_{LJ} and σ_{ij} the distance at which the inter-particle potential is zero. Figure 12 below, illustrates a typical Lennard-Jones plot between pair of atoms and also shows the position of ε and σ.

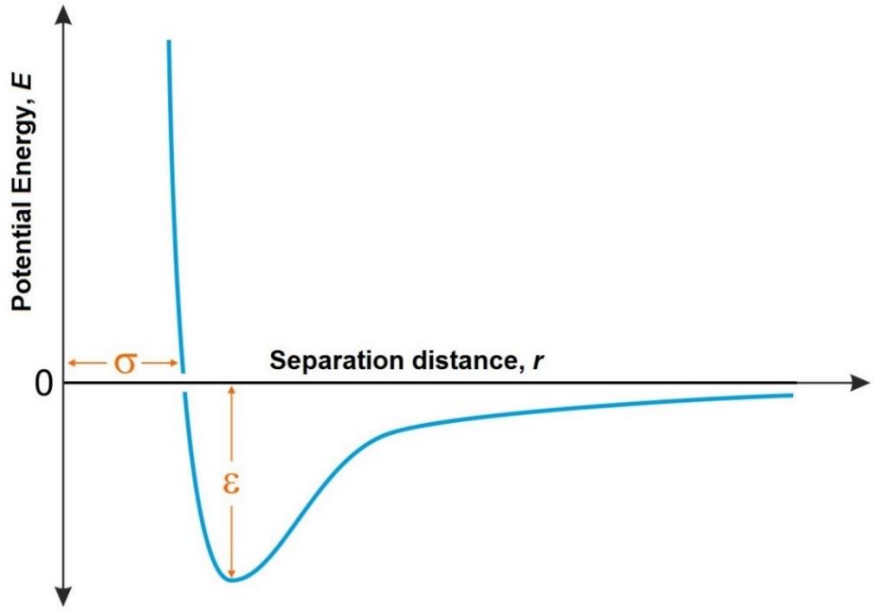

Figure 12: Plot of a typical Lennard-Jones 6-12 potential.

2.2.6 Coulomb interactions. Some models also calculate the potential energy due to the electronegativity between the atoms, thus requiring the addition of the electrostatic terms [1], [2], [8], [9], [20], [38]. The potential energy for this interaction is calculated using Equation (44) below:

$$E_{AB} = \frac{1}{4\pi\varepsilon_o} \sum_{\substack{i,j \\ i<j}} \frac{Q_i Q_j}{R_{ij}} \tag{44}$$

where, in Equation (44), Q_i represents the point charges of atoms i, R_{ij} is the distance between the atoms and ε_o (the permittivity of free space) equals 8.85419×10^{-12} C^2 N^{-1} m^{-2}.

2.3 Force-Fields

Force-fields are used in molecular simulations to carry out the potential energy calculations and contain all the necessary information relating to atoms and groups that make up a molecule. Equation (38) represents a typical form of what is referred to as

class I force-field. Class I force-fields are typically designed based on the harmonic motion that is derived from Hooke's law. Such force-fields are typically used to carry out simulations based on biological molecules, such as proteins and DNA, in order to study their folding and supercoiling properties. Furthermore, several class I force-fields have also been developed to study the thermophysical properties of hydrocarbons, ionic liquids and refrigerants [14].

Class II force fields contain additional terms that account for the coupling of different potentials, such as between bonds stretching and inversion potential. Moreover, in contrast to the use of Hooke's law; class II force-fields tend to use the anharmonic Morse potential or other more accurate descriptors, in order to provide a more realistic picture of the vibrational and stretching phenomena within molecules. Lastly, class III force-fields are also being developed that explicitly include terms for polarization [14]. However, it is to be noted that the thermophysical properties are almost always predicted using class I force-fields and other classes of force-fields are rarely used.

Many different types of force-fields exist in the field of molecular simulation that are used according to the need of the system. For example, some force-fields are modified as per the solution properties against amino acids [15], [21]. Some of the common force-fields found in molecular simulation computational codes are listed in the sub-sections below.

2.3.1 AMBER. The Assisted Model Building and Energy Refinement or AMBER force-field was developed by Cornell et. al. [53] for conducting MD simulations on proteins, nucleic acids, and other organic molecules. Their work showed good accuracy in reproducing the interaction energies, solvation, and conformational energies of small molecules.

2.3.2 COMPASS. Condensed-phase Optimized Molecular Potentials for Atomistic Simulation Studies or COMPASS, a class II force-field was first developed by Sun [54] in 1998. The COMPASS force-field was primarily developed to study small organic and inorganic molecules and polymers. Additionally, COMPASS provides parameters for the 9-6 Lennard-Jones potential instead of the 6-12 [54].

2.3.3 TraPPE. Transferable Potentials for Phase Equilibria or TraPPE is a force-field developed for studying phase equilibria of n-alkanes, branched alkanes, ketones, aldehydes and alcohols [55].

Some other force fields such as OPLS (Optimized Potentials for Liquid Simulations) for studying organic molecules and peptides [56] and carbohydrates [57], ReaxFF (a Reactive force-field for studying reactions) [58] and CHARMM (Chemistry at Harvard Molecular Mechanics) for studies involving proteins and peptides [59] are also available.

2.4 Simulation Techniques

2.4.1 Interaction potentials. In order to save on computing power, some force fields use simplified interaction potentials [21]. There are three such approaches, namely: the All-Atoms (AA) [22] or atom-atom [15], [16] model, United Atom (UA) model [16], [21], [22], and the Anisotropic United Atom (AUA) [21], [37] model. These models consider different force centers in order to model an atom or a group of atoms. Figure 13 provides a depiction of the three different models.

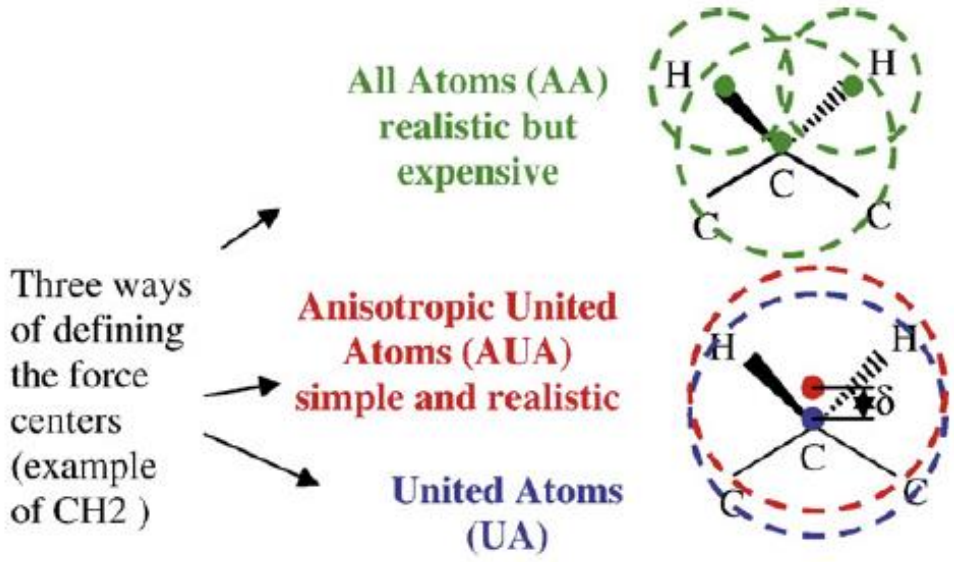

Figure 13: Three different models of determining the force centers [22].

The most realistic and accurate model is the AA model that has the force center on each individual atom. However, this model is considered to be highly intensive in terms of calculations among the three, as it requires more computing power [16], [22]. The UA model considers the force center to be at the main atom of a group of atoms.

For example, in a CH_3 methyl group, the force center is located on the carbon atom [16], [21], [22]. The AUA model is similar to the UA model, but with the force center located at an intermediate position rather than on the main atom [22].

2.4.2 Periodic boundary conditions. Because of speed and memory limitations in a small computer, molecular simulations are usually run with a system containing hundreds to tens of thousands of molecules. The simulations, therefore, would simulate a very small aerosol drop rather than a bulk fluid. This would result in the ratio of the number of molecules at or near the surface to the number of molecules in the bulk liquid be greater when compared to the same ratio for a large amount of liquid. Hence, causing the simulations to provide inaccurate results [14]–[16], [29].

In order to overcome this problem, periodic boundary conditions are applied which makes the system think that it is larger than it actually is. During the simulation, the actual simulation box is surrounded by its periodic images. Thus, if a molecule exits from one side of the simulation box, its copy enters from the periodic image into the main simulation box from the opposite side [14]–[16], [29]. Figure 14 shows a typical 2D representation of the periodic boundary condition.

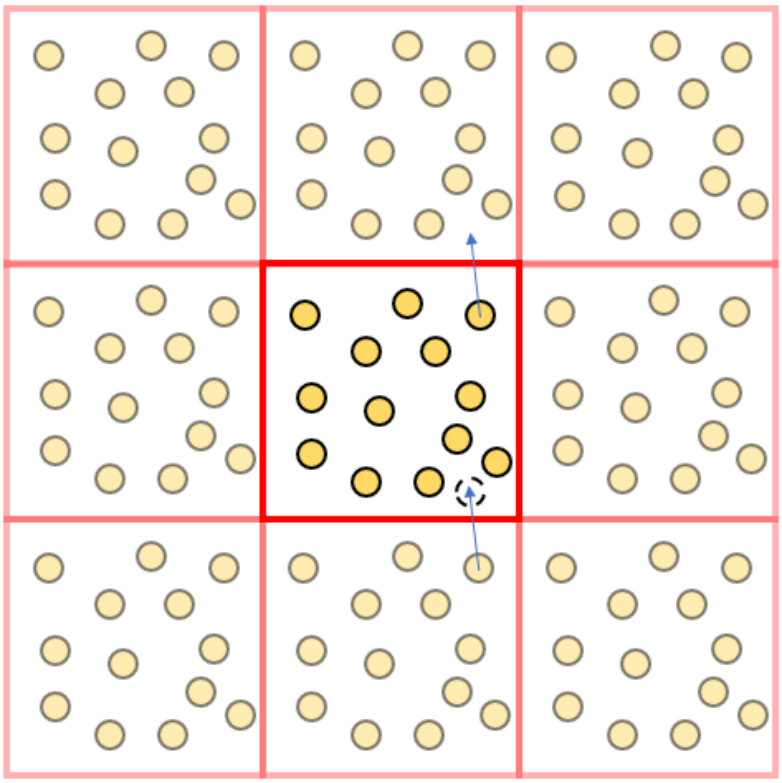

Figure 14: Periodic boundary condition.

2.4.3 Minimum image convention and cut-off radius. A minimum-image-convention, as shown in Figure 15, is used along with the periodic boundary conditions. Hence, when calculating the interaction between molecules, a cut-off distance of one-half the length of the box is typically used. This is done to ensure that one molecule does not interact with copies of the same molecule in other periodic boxes, which would introduce a false periodicity and also drastically increase the computational time [14]–[16], [29].

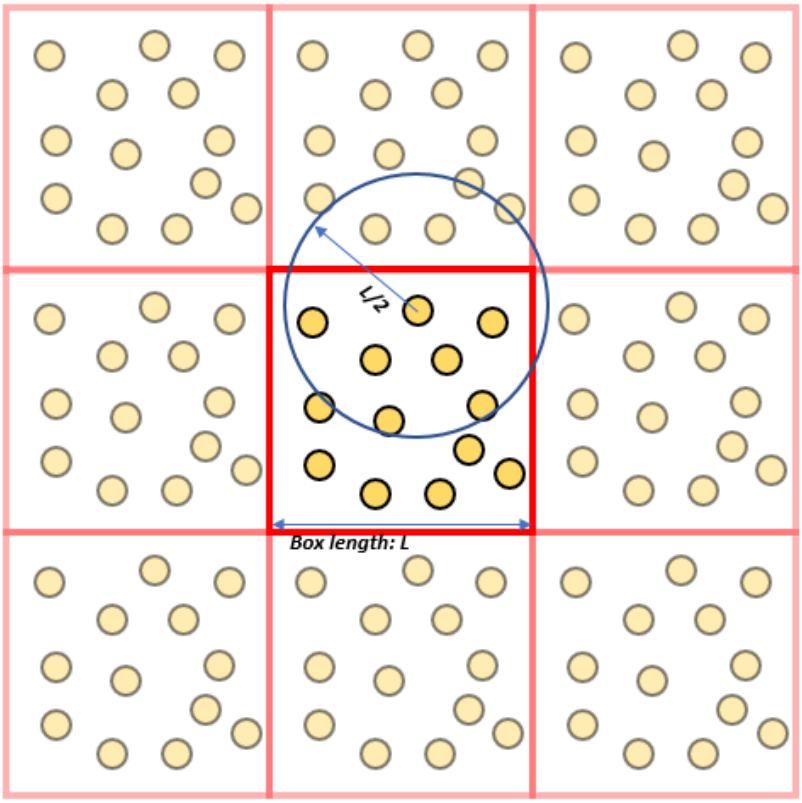

Figure 15: Minimum image convention.

For simulations of systems that contain a large number of particles; it may be necessary to use a cut-off radius for the LJ potential in order to reduce the computational time. Such measure is usually taken since the pair potential energy is negligible for particles that are far away. The cut-off radius for LJ potential is typically taken to be 2.5σ [60], [61], however, a cut-off radius of more than 2.5σ has been reported [36], [37], [52], [62]. This results in the LJ truncated potential (see Figure 15), with the conditions given in Equation (45) below [63]:

$$E_{LJ} = \begin{cases} LJ(r), & r < r_{cut-off} \\ 0, & r \geq r_{cut-off} \end{cases} \tag{45}$$

Because of the sudden truncation, the potential near the cut-off radius is similar to a step-wise function. Hence, in order to allow the LJ potential reach zero smoothly; a switching function $S(r)$ is used as shown in Equation (46) [63]:

$$S(r) = \frac{[r^2{}_{out} - r^2]^2[r^2{}_{out} + 2r^2 - 3r^2{}_{in}]}{[r^2{}_{out} - r^2{}_{in}]^3} \tag{46}$$

where r_{out} is the outer radius cut-off, while r_{in} is the inner radius cut-off. The conditions for using the cut-off radius with the switching function is displayed in Equation (47) [63]:

$$E_{LJ} = \begin{cases} LJ(r), & r < r_{in} \\ S(r) * LJ(r), & r_{in} \leq r < r_{out} \\ 0, & r \geq r_{out} \end{cases} \tag{47}$$

Figure 16 depicts the comparison between the three types of LJ potentials.

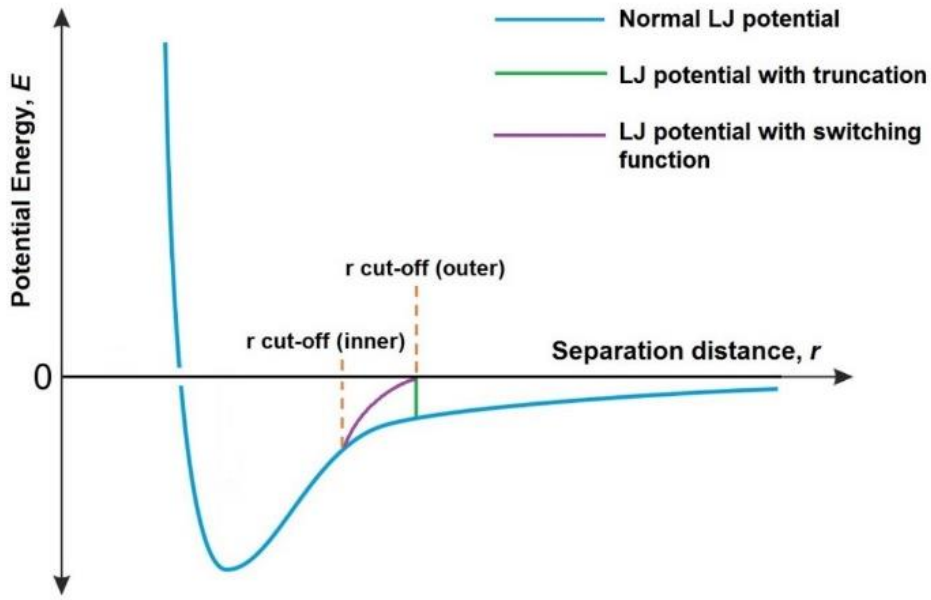

Figure 16: LJ potential with truncation and switching functions.

2.5 Monte Carlo Simulations

The MC method is a stochastic method, i.e., it uses probability functions to construct a mathematical model simulating a real system in order to determine numerical results. MC was first used in the 1940s by John von Neumann, Stanislaw Ulam and Nicholas Metropolis, who were working on the nuclear weapon project: the

Manhattan Project. The use of the MC method allowed scientists to construct mathematical models in order to solve a series of algorithms that were too complex to be solved analytically [64].

The basis of the MC method is to generate successive configurations of each particle or molecule in the system by a probability or a statistical method, such that the probability distribution of the desired statistical ensemble is met [14], [15], [21], [28], [29]. Figure 17 below, provides a summary of the moves that can be performed in a MC simulation. Under a given set of conditions, there could be several combinations of the moves that are displayed in Figure 17.

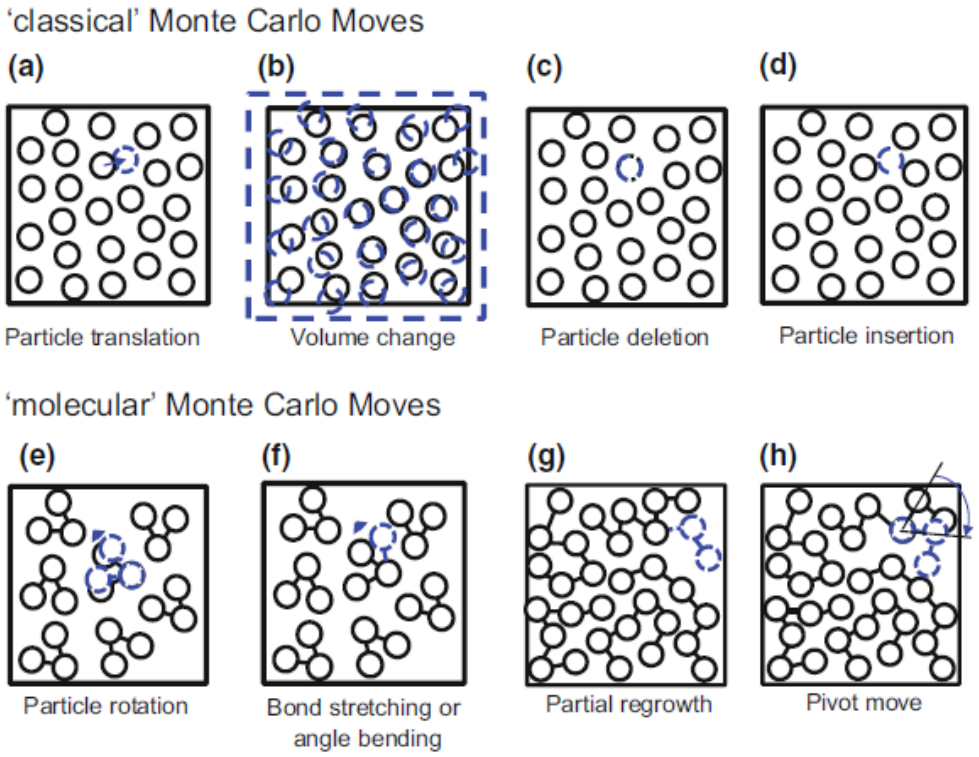

Figure 17: Moves available in a MC simulation [14].

Each MC move (i.e. the change in the configuration) is generated by applying an elementary change. For the system to meet the desired equilibrium distribution, only the micro-reversibility criterion needs to be observed [22], which states that the flux of configurations from state *i* to state *j* is equivalent to the inverse flux from state *j* to state *i* (see Equation (48) [14], [15], [22], [28], [29]). This results in what is known as the "Metropolis method".

$$\wp_i \pi_{ij} = \wp_j \pi_{ji} \tag{48}$$

where $\wp_i$ is the probability distribution of configuration *i*, proportional to the Boltzmann weight for a given ensemble, for example, for the canonical ensemble this is exp(-βE) and π_{ij} is the transition probability from configuration *i* to *j* [14], [15], [22], [28], [29].

The microscopic reversibility criterion is then used to determine appropriate transition probability from state *i* to *j* in a single MC move. This condition is satisfied by the Metropolis algorithm as displayed in Equation (49) [14], [15], [22], [28], [29]:

$$\pi_{ij} = \min\left[1, \frac{\wp_j}{\wp_i}\right] \tag{49}$$

For example, in the canonical ensemble, the test configuration for a particle *k*, would be accepted when the following Equation (50) is satisfied [14], [15], [22], [28], [29]:

$$\pi_{ij} = \min\left[1, exp\left(\beta \Delta E_k^{i \to j}\right)\right] \tag{50}$$

where ΔE_k is the change in the potential energy of the system when changing from configuration *i* to configuration *j*.

In the Metropolis scheme, the transition probability π_{ij} comprises the probability of suggesting the transition α_{ij} and the probability of accepting this transition, acc_{ij}, as shown in Equation (51) [14], [15], [28], [29].

$$\pi_{ij} = \alpha_{ij} \cdot acc_{ij} \tag{51}$$

A move is accepted when the configurational energy in state *j* is lower than that in state *i* (i.e. if $\wp_j$ is greater than $\wp_i$). If the energy in state *j* is higher, then a random number, R_{andom}, is generated that is between 0 and 1. If R_{andom} is less than the ratio of the configuration energies, the move is accepted, otherwise the move is rejected [14], [15], [28], [29]. Equations (52) and (53) summarize the scheme as provided in the Metropolis method [14], [15], [28], [29]:

$$\pi_{ij} = \begin{cases} accept\ move, & \wp_i < \wp_j \\ reject\ move, & \wp_i > \wp_j \end{cases} \tag{52}$$

$$if\ \wp_i > \wp_j, generate\ R_{andom}[0,1]$$

$$\pi_{ij} = \begin{cases} accept\ move, & R_{andom}[0,1] < \dfrac{\wp_j}{\wp_i} \\ reject\ move, & R_{andom}[0,1] > \dfrac{\wp_j}{\wp_i} \end{cases} \tag{53}$$

Additionally, the Metropolis method creates what is known as the Markov change of states. In such a condition, the transition probability π_{ij} is only dependent on states *i* and *j* and not the states that preceded before them [14]. Furthermore, the Metropolis algorithm may then be adapted to generate favorable configurations more frequently in order to reduce the computational time. These statistical biases are now standard in MC simulations and can handle systems with flexible linear chains [65], flexible branched molecules [66] and flexible cyclic molecules [67]. One such bias is known as the configurational bias where a molecule is grown segment-by-segment, in a way to minimize the energy as discussed for Metropolis method. The configurational bias is the most commonly used bias in MC simulations. Figure 18 below depicts the use of the configurational bias for a lattice:

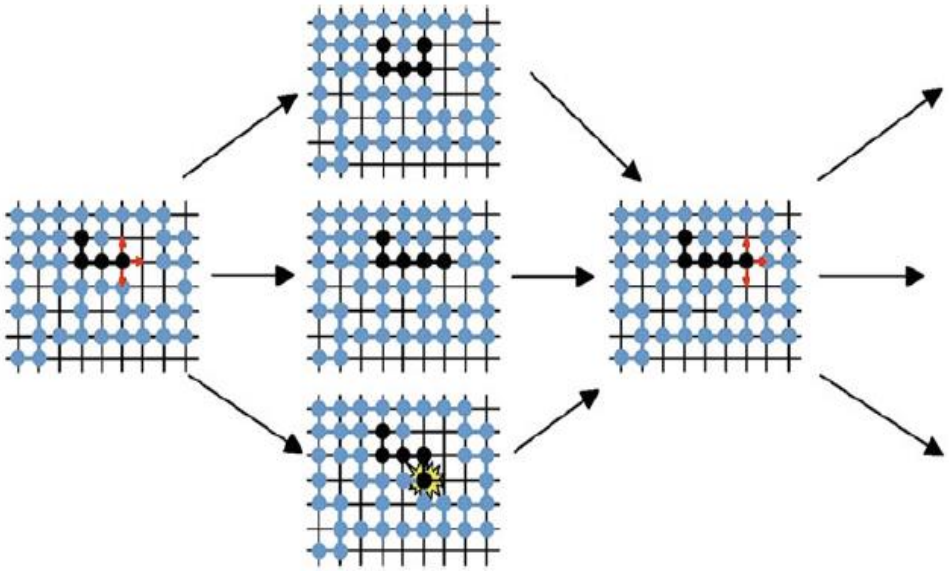

Figure 18: Configuration bias for a molecule on a lattice model [14].

In Figure 18, there are three possible moves the molecule can grow about. Of the three possibilities as shown in the middle three images, only the first two are possible. The third possibility would maximize the energy because of the presence of a molecule, thus showing that the molecule cannot grow in the stated direction [14], [68].

Lastly, another type of bias is the oriental bias where a molecules orientation is continuously displaced based on the force center until the orientation becomes acceptable [14].

2.6 Molecular Dynamics Simulations

Molecular dynamics (MD) is dynamic rather than artificial [19], [51]. MD follows the time evolution of a system by applying and numerically integrating Newton's law of motions (Equation (54)) [18] at regular time increments (typically in the order of 10^{-14} s) for a set of *N* particles in the phase space [14], [19], [22]. This results in the particle's trajectory to be specified according to the variation in velocity and position with time. However, because of the increase in the number of equations that need to be solved, MD is more computationally intensive than MC.

$$\boldsymbol{F}_A = m_A \frac{d^2 \boldsymbol{R}_A}{dt^2} \tag{54}$$

where, m_A is the mass of particle *A*, and $\boldsymbol{R_A}$ is the position vector of the particle *A*. Hence, the second-order differential term in Equation (54) represents acceleration.

However, using Equation (54) and the Newtonian approach in general, is only suitable for Cartesian coordinate systems. In order to study more dynamic systems, additional forces would need to be defined, but in most systems these forces are unknown [18].

In order to overcome this problem, convenient formulations exist that are not tied to any one coordinate system [18]. One common formulation is the Hamiltonian. Considering a set of *N* particles, there will be 6N degrees of freedom in the Hamiltonian, as for each particle, the momenta and position would need to be calculated in a 3D space in order to specify the trajectories of the particles. Equation (55) describes the Hamiltonian of the system *H* [18]. **r** and **p** represent the positions and momenta of the particles, respectively. Furthermore, Equations (55)-(57) collectively represent the Hamiltonian equations of motions [15], [18], [29].

$$H(\boldsymbol{r}^N, \boldsymbol{p}^N) = \sum_i \frac{\boldsymbol{p}_i^2}{2m_i} + E(\boldsymbol{r}^N) \tag{55}$$

$$\dot{r}_i = \frac{\partial H}{\partial p_i} = \frac{p_i}{m_i} \tag{56}$$

$$\boldsymbol{p}_i = -\frac{\partial H}{\partial \boldsymbol{r}_i} = -\nabla_{\boldsymbol{r}_i} E(\boldsymbol{r}^N) \tag{57}$$

The system of equations can be solved numerically using integrators like Verlet-based or Gear-based predictor-corrector algorithms. Equations (58) and (59) represent the velocity Verlet algorithm which is the most widely used algorithm [14], [15], [18], [19], [22], [51]:

$$\boldsymbol{r}_A(t + \Delta t) = \boldsymbol{r}_A(t) + \left(\frac{d\boldsymbol{r}_A}{dt}\right)_t \Delta t + \frac{1}{2}\left(\frac{d^2\boldsymbol{r}_A}{dt^2}\right)_t (\Delta t)^2 \tag{58}$$

$$\boldsymbol{v}_A(t + \Delta t) = \left(\frac{d\boldsymbol{r}_A}{dt}\right)_t + \frac{1}{2}\left(\frac{d^2\boldsymbol{r}_A}{dt^2}\right)_t \Delta t + \frac{1}{2}\left(\frac{d^2\boldsymbol{r}_A}{dt^2}\right)_{t+\Delta t} \Delta t \tag{59}$$

In MD, the temperature is directly proportional to the average kinetic energy of the systems as shown by Equation (60) below [51], [69]:

$$T = \frac{2}{3k_B}\langle \frac{1}{N}\sum_{i=1}^{N} \frac{|\boldsymbol{p}_i|^2}{2m_i} \rangle \tag{60}$$

where $\langle\ \rangle$ represents the average of the ensemble, N is the total number of particles, m_i is the mass of particle i and k_B is the Boltzmann constant.

In order to keep the system at constant temperature and not allow fluctuations due to changes in the kinetic energy, a heat-bath at the desired temperature is applied to act as a thermostat. Many different thermostats are available to be used in the MD simulations, such as the Anderson thermostat [70]. However, the most commonly used thermostat is the Nose-Hoover. This is because the Nose-Hoover allows a user to perform deterministic calculations in MD at constant temperature. Equation (61) below displays the Nose-Hoover thermostat which needs to be conserved in order to keep the temperature constant [29]:

$$H_{Nose-Hoover} = \sum_{i=1}^{N} \frac{\boldsymbol{P}_i{}^2}{2m_i s^2} + E(\boldsymbol{r}^N) + \frac{\boldsymbol{p}^2}{2Q} + Lk_B T(\ln(s)) \tag{61}$$

where the first two terms in Equation (61) represent the kinetic and potential energy terms respectively. The *s* term is the time scale parameter. *L* is the number of the degrees of freedom, which in the case of the canonical ensemble is 3N+1, due to the addition of the extra degree of freedom coming from the parameter *s*. Lastly; *Q* is the strength of the coupling between the system and the heat bath and should be set carefully. If *Q* is too large, then there will be weak coupling resulting in poor temperature control, conversely if *Q* is too small, then the temperature will keep on fluctuating [29].

Pressure in a MD simulation of a homogeneous system is studied according to Equation (62) [69]:

$$P = \langle \frac{Nk_BT}{V} + \frac{1}{3V}\sum_{i=1}^{N-1}\sum_{j>i} r_{ij}.f_{ij} \rangle \tag{62}$$

where *r* is the location of particles and $r_{ij} = r_i - r_j$. f_{ij} is the force applied by particle *j* on particle *i*.

Similar to the thermostat, a barostat is also required in order to keep the pressure constant during the simulation. Again, coupling the system to a constant pressure bath (similar to a piston) can be implemented like the coupling of a constant temperature bath. By adding an extra term to the equations of motion, the pressure change is affected as displayed in Equation (63) [71]:

$$\left(\frac{dP}{dt}\right)_{bath} = \frac{P_o - P}{\tau_P} \tag{63}$$

where τ_P is the time constant, P_o is the pressure of the bath and *P* is the pressure of the system. Moreover, applying a proportional coordinate scaling, related to the volume scaling, minimizes the local disturbances. This is shown in Equation (64) (in the form of αx that is added to $\dot{x} = v$) with the volume change shown in Equation (65) [71]:

$$\frac{dx}{dt} = v + \alpha x \tag{64}$$

$$\frac{dV}{dt} = 3\alpha V \tag{65}$$

The pressure change is related to isothermal compressibility (κ_T) as illustrated in Equation (66) [71]:

$$\frac{dP}{dt} = -\frac{1}{\kappa_T V}\frac{dV}{dt} = -\frac{3\alpha}{\kappa_T} \tag{66}$$

Substituting Equation (63) into Equation (66) gives the following Equation (67) in terms of α:

$$\alpha = -\frac{\kappa_T}{3\tau_P}(P_o - P) \tag{67}$$

where κ_T is the isothermal compressibility that only requires a general value, as the dynamics of a solution are largely unaffected due to the inaccuracy of κ_T [71].

Equation (67) is now substituted into Equation (64) to give Equation (68) as shown below. This equation represents the proportional scaling of coordinates, *x* and box length *l*, with a time step change of Δt from *x* to μx and *l* to μl [71].

$$\mu = 1 - \frac{\kappa_T \Delta t}{3\tau_P}(P_o - P) \tag{68}$$

2.7 Thermophysical Properties from Molecular Simulations

2.7.1 Shear viscosity. The viscosity of hydrocarbons is an important property since products like lubricants depend on how temperature and pressure affect viscosity, which would lead to their use in a fitting application. Since viscosity is a dynamic property, only MD can be used for its prediction [22], [69].

2.7.1.1 Equilibrium molecular dynamics. One way to calculate viscosity is to use the Green-Kubo relationship in Equilibrium Molecular Dynamics (EMD), as shown in Equation (69), in which $\sigma_{xy}(t)$ is the component of the pressure tensor at equilibrium time [69], [72]:

$$\eta = \frac{V}{k_B T}\int_0^\infty \langle \sigma_{xy}(t)\sigma_{xy}(0)\rangle dt \tag{69}$$

where, η is the viscosity to be calculated, and *V* is the volume of the system. The infinity on the integral represents the system at the time of equilibrium. Hence, simulations involving EQMD need to be run for long periods of time in order to achieve equilibrium values of viscosity. Additionally, the use of the Green-Kubo relationship, allows for the inclusion of inaccuracies due to it's correlative nature.

The results for the xylene isomers at a temperature of 323 K for different pressures are presented in Figure 19 for two different force fields, derived from the OPLS [73] and AUA potentials [22], [37]. Furthermore, the results obtained from the simulations are compared to the experimental data.

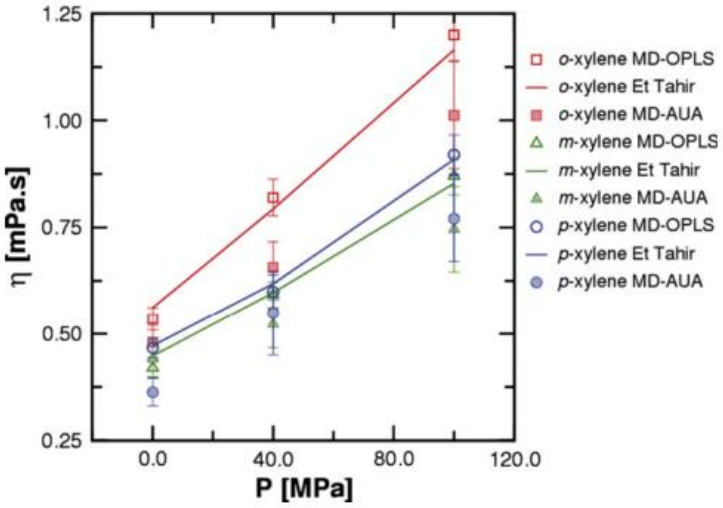

Figure 19: MD results for the xylene isomers [22].

Figure 19 illustrates the difference between the two force-fields. As it can be observed, the OPLS force-field produces results much closer to the experimental results, with a maximum deviation of less than 6% [73]. On the other hand, the AUA model greatly underestimates the viscosity of all the isomers. This is because, unlike OPLS, the AUA model does account for the electrostatic interactions between the molecules. Nonetheless, the AUA model does predict an increase in viscosity with pressure which is consistent with the experimental data [22].

2.7.1.2 Non-Equilibrium Molecular Dynamics (NEMD). Compared to use of Green-Kubo formalism, NEMD is considered to be more accurate since the statistical uncertainty with the use of a correlation is reduced [74]. Furthermore, NEMD requires fewer particles and simulation time as compared to EMD [75]. There are different methods by which a NEMD simulation can be carried out. The first method is similar to that of a Couette flow, whereby the periodic boxes surrounding the main simulation box at the top and bottom are moved at opposite velocities, resulting in shear stress being applied to the system inside the main simulation box [74], [75]. This method is known as the periodic perturbation method [76]. Figure 20 below represents the shear stress that is applied:

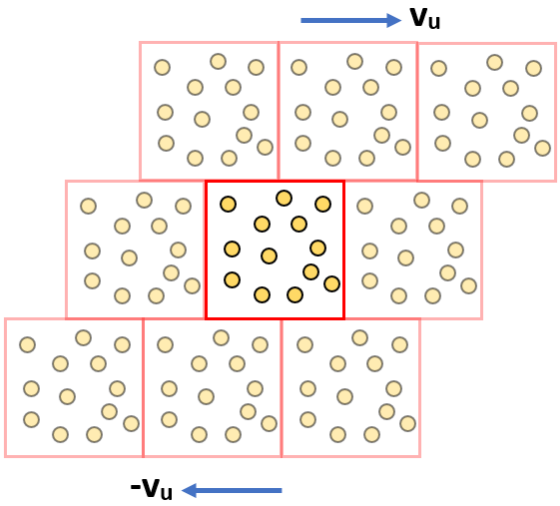

Figure 20: Movement of periodic boxes at top and bottom.

Another method is known as the Muller-Plathe method or reverse NEMD (RNEMD) method, where momenta between two particles at different positions in a simulation box are exchanged. Hence, resulting in the formation of shear velocity profile which can then be used to calculate the shear viscosity [77], [78].

2.7.2 Critical properties. Unlike other thermophysical properties, a problem arises with the prediction and calculation of the critical properties. This is because no relationships exist in statistical mechanics that can calculate the critical properties directly from the available equilibrium energy or any other variables. Furthermore, approaching the critical point in a molecular simulation results in the density of the vapor and liquid phase to be identical [29]. Hence, the methods usually employed require the measurement of density at temperatures lower than the critical temperature and then use the scaling laws to determine the critical properties. These techniques are discussed in more detail in the following sections, for both the MC and MD methods.

2.7.2.1 ***Critical properties from Monte Carlo.*** The MC method has been extensively used to calculate the critical properties of a system through the simulations of phase equilibria.

2.7.2.1.1 *Gibbs ensemble.* The most common method to predict the critical properties by simulating the phase equilibria is through the Gibbs ensemble method. In the early stages of the use of Gibbs ensemble, simple systems, such as spherical Lennard-Jones particles, were studied. Later, more complex systems such as alcohol-water mixtures and polyatomic hydrocarbons were studied [79]. The general algorithm

for the Gibbs ensemble is displayed in Figure 21. Two boxes (one for liquid phase and the other for the vapor phase) are used in this ensemble where only the initial densities and temperature are provided. The first step is to randomly displace a particle in each box. The second step is then to change the volume of the boxes, such that the total volume of the system is kept constant. This is done randomly, but in a correlated manner. The final step involves exchanging a particle from one box to the other, but keeping the total number of particles constant as in the initial system [80]. Probability functions from statistical mechanics are used to decide which box would receive the particle as mentioned in Equations (52) and (53) in the preceding sections.

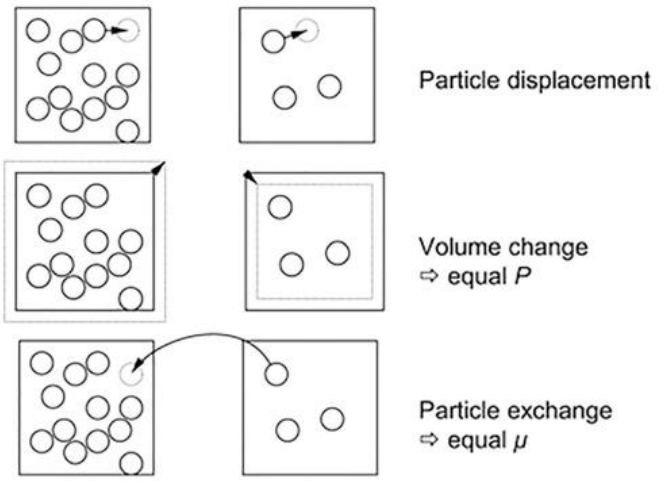

Figure 21: Steps in the Gibbs ensemble [80].

The Gibbs ensemble method has also been used to simulate various hydrocarbon systems in order to find the critical temperature and density. In one of the methods [37], MC moves of the molecules involved were translations, rigid body rotations, transfers and volume changes. The simulations were carried out for 150 molecules and the Anisotropic United Atom (AUA) model was used for the pair potentials. Furthermore, the simulations were performed at temperatures below the critical temperature, because at the critical point, the MC method is unable to reach equilibrium due to low acceptance ratio of transfer moves [36], [37].

After the completion of the simulations the critical temperature and density were then obtained by fitting the critical scaling law (Equation (70)) and the law of rectilinear diameters (Equation (71)), respectively [37].

$$\rho_l - \rho_v = \lambda(T_c - T)^{0.3265} \tag{70}$$

$$\frac{1}{2}(\rho_l + \rho_v) = \rho_c + \gamma(T - T_c) \quad (71)$$

where ρ is the density at a particular temperature, T, and the subscripts l, v and c represent the liquid, vapor, and critical properties, respectively. λ and γ are constants that are fit with the available simulation data.

The results obtained from these simulations are displayed in Table 2. As evident from Table 2, the percentage deviations between the simulated values and the experimental values is less than 5% in all cases, making the results acceptable. Additionally, the average absolute deviations are 1.1% and 2.7% for critical temperature and density, respectively. These deviations could be attributed to the choice of the pair potential model and therefore, could be reduced if a more accurate model is used.

Table 2: Results using the Gibbs ensemble Monte Carlo technique [37].

	T_c (K)			**ρ_c (kg/m^3)**		
	AUA	**Experimental values**	**Percentage Deviation**	**AUA**	**Experimental values**	**Percentage Deviation**
2,3-Dimethylpentane	543	537	1.1	243	255	−4.7
2,4-Dimethylpentane	532	520	2.3	243	240	1.3
***n*-Propylbenzene**	627	638.2	−1.8	281	273	2.9
***n*-Hexylbenzene**	688	698	−1.4	275	274	−1.6
***n*-Propylhexane**	636	639	−0.4	255	265	−3.9
***n*-Propylpentane**	600	596	0.7	254	262	−3.1
***trans*-Decalin**	684	687	−0.5	278	288	−3.4
Tetralin	728	720	1.1	314	322	−2.6
Indan	679	685	−0.9	295	298	−1.2

Although molecular simulations do well in predicting the critical densities and temperatures; it is quite difficult to model the vapor pressure of a system. Hence, alternative methods, such as the Antoine Equation, are used [34]. Another method is to use the modified form of Rackett's Equation as done by Vetere to calculate the critical pressure from the critical density and temperature as modelled by the simulation [34]. Equation (72) presents the equation for calculating the critical pressure [34].

$$P_c = \frac{RT_c\rho_c}{MW}\left(\frac{\rho_c}{\rho_l}\right)^{\left(1-\frac{T_i}{T_c}\right)^{-\frac{2}{7}}} \quad (72)$$

where, R is the gas constant, MW is the molecular weight and T_i is the temperature at the liquid density.

2.7.2.1.2 *Histogram reweighting method*. The second technique that can be used to study the phase equilibria is the Grand Canonical MC method with histogram reweighting. In this method, the density is allowed to vary, while the chemical potential is held constant. Equilibrium is achieved when the chemical potentials of both phases reach a constant value. In theory, the probability distribution, which is a function of total energy, E, should exhibit two peaks at a given temperature and chemical potential because of the presence of two phases. Hence, separate simulations for liquid and vapor phase are conducted that are just below the critical point, after which the histogram reweighting is applied to combine the results and predict the critical properties [14]. Moreover, unlike the Gibb's ensemble method where the simulations have to be carried out below the critical point; it is possible to derive the critical properties of a system using histogram reweighting method by extrapolation of results from a simulation that is conducted close to the critical point [81].

GCMC has been used with histogram reweighting to find the phase diagrams of hexadecane-CO_2 mixture. Binodal curves for pure species were also found as displayed in Figure 22 below.

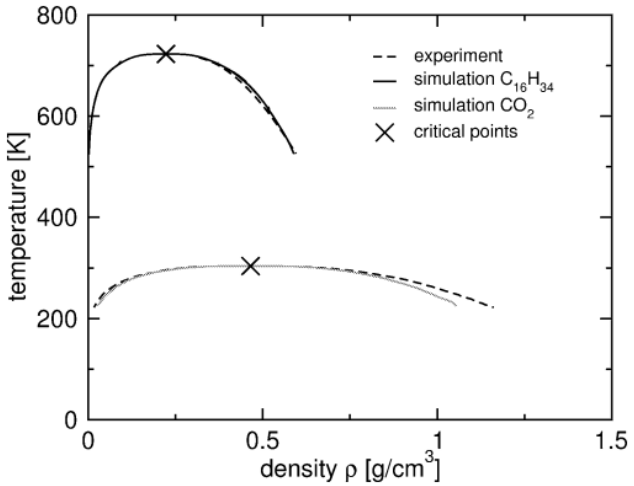

Figure 22: Binodal curves for pure hexadecane and CO_2 [82].

From Figure 22, it can be observed that the simulated binodal curve of hexadecane is more in agreement with the experimental value as compared to the binodal curve for CO_2. The reason for the disagreement between the experimental and simulated binodal curves is because of neglecting the electronegative charges in the pair potential model CO_2 [82].

Additionally, the histogram reweighting technique with the Gibbs ensemble method is slowly being used more often than standalone Gibbs ensemble, as they predict the critical points more accurately and efficiently [36]. In histogram reweighting for Gibbs ensemble, a histogram of particle number and energy is collected. Histogram reweighting techniques are then applied, along with finite size scaling, to extract thermodynamic properties from the probability distribution of density [83]. Figure 23 shows the predicted results of having a specific density at a probability distribution from the coexistence curves of CO_2, generated by Gibb's ensemble simulations.

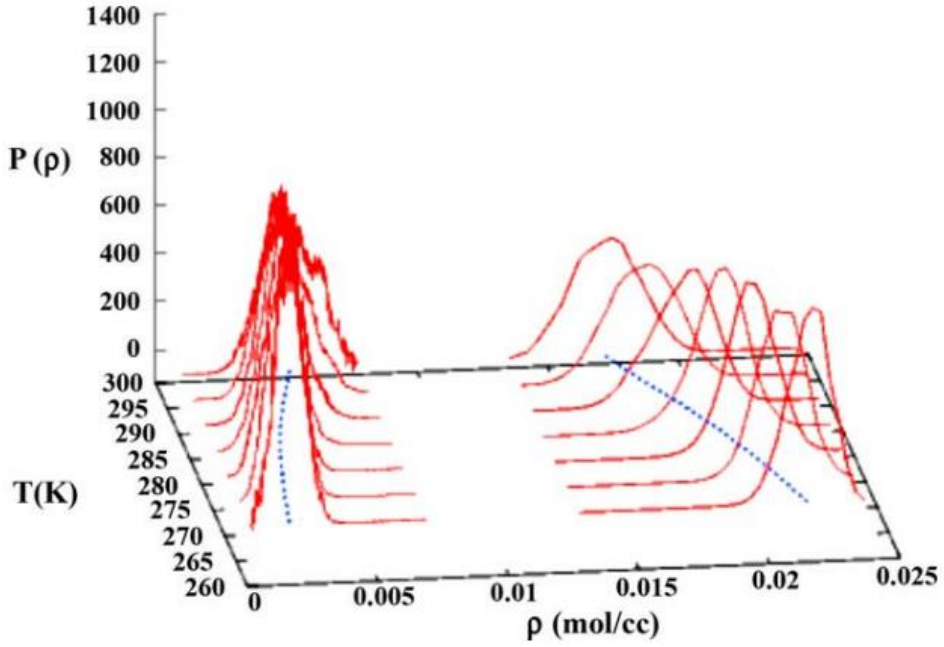

Figure 23: Probability distribution of having a specific density at different temperatures extrapolated using only 3 Gibbs ensemble simulations [83].

2.7.2.1.3 *Gibbs-Duhem integration.* In this method, the famous Gibbs-Duhem equation is used [84], as shown in Equation (73) below:

$$S_m dT - V_m dP + \sum_i x_i d\mu_i = 0 \tag{73}$$

where the S_m and V_m are the molar entropy and volume, respectively. μ_i is the chemical potential of species i, while x_i is the mole fraction. For a pure system containing the vapor (I) and liquid (II) phases, the Gibbs-Duhem equation is given by Equations (74) and (75):

$$S_{m,I}dT_I - V_{m,I}dP_I + d\mu_I = 0 \tag{74}$$

$$S_{m,II}dT_{II} - V_{m,II}dP_{II} + d\mu_{II} = 0 \tag{75}$$

Using the thermodynamic criteria of phase existence that sets the change in temperature, pressure and chemical potential to be equal, Equations (74) and (75) can be subtracted to yield Equation (76), as depicted below [14], [84]:

$$\left(\frac{\partial P}{\partial T}\right) = \frac{S_{m,II} - S_{m,I}}{V_{m,II} - V_{m,I}} = \frac{H_{m,II} - H_{m,I}}{T\left(V_{m,II} - V_{m,I}\right)} \tag{76}$$

The right-hand side of Equation (76) is the Clapeyron equation and is suggested to be evaluated through the use of molecular simulations (MD and MC [84]). Additionally, unlike the Gibbs ensemble MC, the Gibbs-Duhem integration can be used to conduct vapor-liquid simulations, as well as solid-liquid equilibria. Moreover, as compared to the Gibbs ensemble simulations that provide a single point on the phase diagram per simulation, the Gibbs-Duhem integration method provides a series of points. However, it is to be noted that at least one point on the coexistence curve is required to be known at the start of the simulation for the Gibbs-Duhem integration [14].

2.7.2.2 *Critical properties from molecular dynamics*

2.7.2.2.1 *Temperature quench molecular dynamics (TQMD).* In this method, a single component liquid-vapor system is considered as shown in Figure 24. The ensemble used is the canonical one, where the number of particles, volume and temperature are held constant. The temperature has to be controlled through the use of a thermostat, an example of which is the Nose-Hoover. Starting from a temperature (a) as displayed in Figure 24, the temperature is lowered abruptly to a new temperature (b). This new temperature must be such that it is within the spinodal envelope of the system. As the system equilibrates at the new temperature, phases of liquids and vapor begin to develop [36].

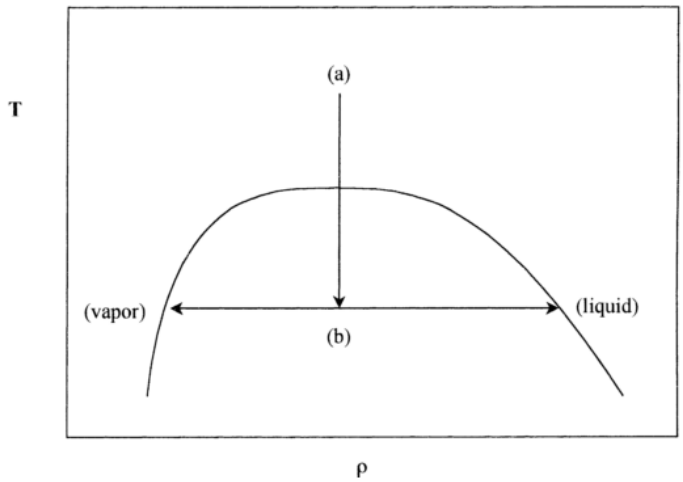

Figure 24: Generalized TQMD method [36].

Figure 25 displays the development of the liquid and vapor phases using TQMD. Snapshot (a) represents the initial state at the Lennard-Jones reduced temperature of $T^* = Tk_B/\varepsilon = 4$ and reduced $\rho^* = \rho\ \sigma^3 = 0.33$. After suddenly reducing the temperature to $T^* = 0.9$, the vapor and liquid phases begin to develop as shown in snapshots (b) – (h). Snapshot (i) shows the equilibrated state, with the vapor phase at the center of the box and the liquid phase on either side.

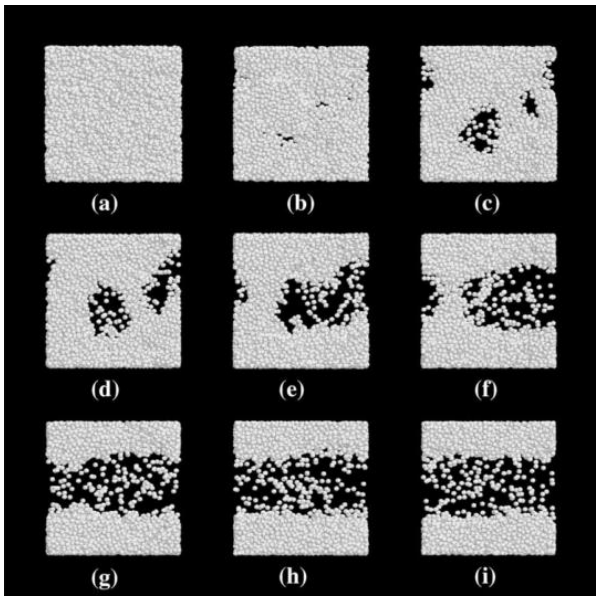

Figure 25: TQMD method. Snapshots show the development of the liquid and vapor phases [36].

2.7.2.2.2 *Volume expansion molecular dynamics (VEMD).* This technique starts by placing a liquid in the box using the canonical ensemble and allow it to equilibrate. After equilibrium is achieved, the volume of the box is suddenly increased, which

decreases the density. This density is present in the unstable region along the line of rectilinear diameters. After a certain amount of time steps, the system separates into a liquid and a vapor phase. Figure 26 shows the snapshot of a box containing propane molecules that has been enlarged along one axis from 15.8 A to 39.51 A. Figure 26 also shows the presence of the two vapor phases on either side of the box, with the bulk liquid phase present in the middle [52].

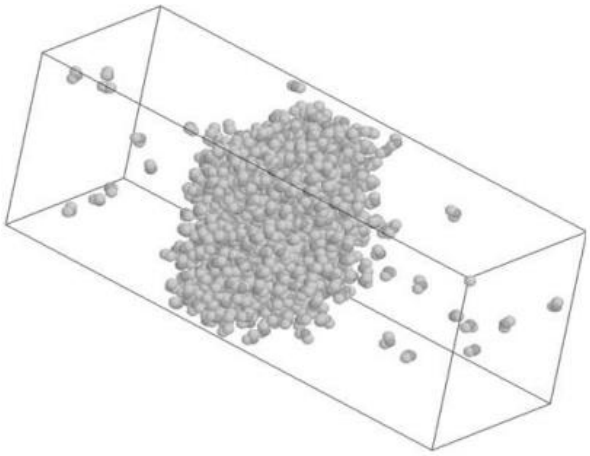

Figure 26: Snapshot of the simulation box of propane at equilibrium at 217 K [52].

Figure 27 also shows the vapor-liquid equilibria of propane obtained from the MD simulations using the VEMD method. In Figure 27, the results show a comparison between simulations performed using MC (squares) and MD (circles).

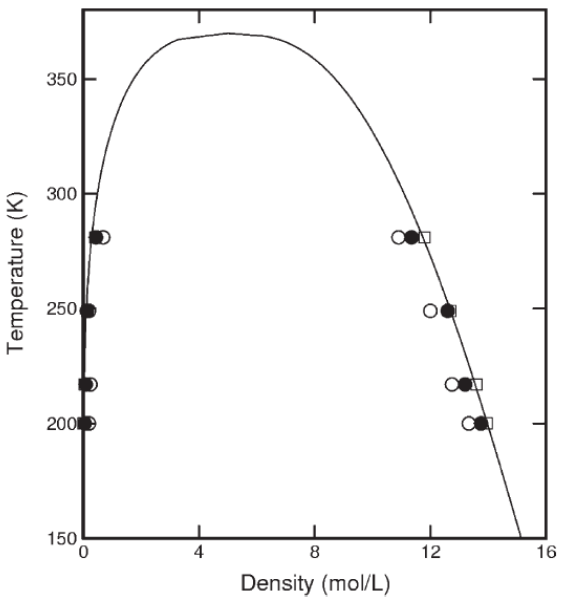

Figure 27: Coexistence curve for propane using MD (circles) and MC (squares) simulations. Black circles represent cut-off of $5.5\sigma CH_2$ while white circles are at a cut-off of $4.5\sigma CH_2$ [52]

2.7.2.2.3 *Gibbs ensemble.* Similar to MC, the Gibbs ensemble method can be used with MD to study the phase equilibria of systems. Gibbs ensemble for MD (GEMD) was first developed in 1995, and uses a fourth positional degree of freedom, ξ, for each particle in the system. This ξ is bounded by zero and one and governs if a particle is supposed to be in the vapor phase (ξ = 0) or liquid phase (ξ = 1). GEMD involves having a constant temperature, volume and number of particles, with the two phases exchanging particles and volumes, to equalize the chemical potential, pressure and temperature [85]. Figure 28 represents a typical scenario of the Gibbs ensemble in MD.

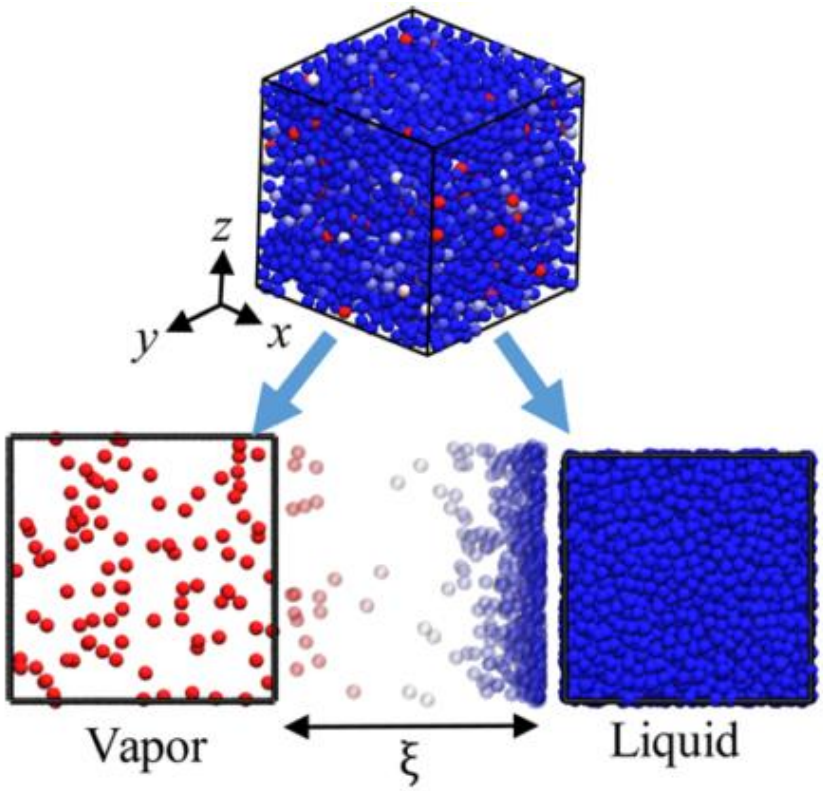

Figure 28: Running the GEMD simulation. Red particles represent the vapor phase (ξ = 0) while blue particles represent the liquid phase (ξ = 1). White particles represent the transition state [85]

The ξ coordinate of each particle, weighs the pairwise potential energy in such a way that the particles that are in the same phase interact strongly with each other and particles that are in opposite phases interact weakly. This modifies the pairwise potential energy, E_{ij} as shown in Equation (77) [85]:

$$E_{ij} = E_{ij}(r_{ij,1})\xi_i\xi_j + E_{ij}(r_{ij,2})(1-\xi_i)(1-\xi_j) \qquad (77)$$

where $r_{ij,1}$ and $r_{ij,2}$ is the distance between the atoms i and j, for phases 1 (vapor) and 2 (liquid) respectively. Additionally, the total potential energy of the system is then calculated as (Equation (78)) [85]:

$$E = \sum_{i<j} E_{ij} + \sum_{i} g(\xi_i) \tag{78}$$

where $g(\xi)$ is an additional potential term, used to make the transition state energetically favorable. The functional form of $g(\xi)$ is displayed in Equation (79) below [85]:

$$g(\xi_i) = w(\tanh(u\xi_i) + \tanh(u(1-\xi_i)) - 1) \tag{79}$$

where u is the steepness and w is the height of the potential, chosen in such a way to give a low, yet nonzero, number of particles in the transition state [85].

2.7.2.3 Hybrid MC/MD. In this method, the Gibbs ensemble formalism is used similar to the MC method, with the presence of two boxes. One box is for the vapor phase while the other is for the liquid phase. However, one key difference is that instead of using MC to predict the position of each particle, the deterministic calculations of MD are used. Thus, allowing for the advantages of both the MC Gibbs ensemble, like ease of applicability, and MD (for example, simulation of dense systems and parallel computing applications) to be present in a single simulation. Moreover, because of the use of MD, dynamics properties can also be determined which is not possible using the MC technique [85].

2.8 Molecular Simulations with Parallel Computing

As stated previously, the most commonly used technique to predict critical properties using molecular simulation is through the use of the Gibbs ensemble MC technique. However, because of the stochastic nature of MC simulations, it becomes difficult to model dense liquids, as the acceptance ratios associated with the insertion and deletion moves for the system have very low acceptance ratios [36]. Hence, with heavier components, conducting Gibbs ensemble MC simulations would take a significant amount of computational time.

In order to overcome this problem, techniques involving MD simulations (as discussed in the previous sections) to predict critical properties have been developed.

This is because MD, (unlike MC) can be easily programmed to run on parallel computing systems, i.e. supercomputers. Although efforts have been made to make MC simulations run with parallel computing, the result is still far from being accurate and simple enough to be able to be applied in research [86].

In parallel computing, a task is broken down into discrete parts or fragments that are then fed to different processors to be solved simultaneously. The processors in this case could be multiple cores on a single central processing unit (CPU) or multiple CPUs on different computers [87].

Therefore, with the aid of parallel computing, the simulations for MD can have significantly shorter computational times that would aid in research as a greater number of simulations with higher time steps and with complex systems could be conducted. This would be especially true in the future, where classical CPUs with higher number of cores would be commercially available leading to faster processing times.

Apart from the use of classical CPUs; there has been rapid developments in the field of quantum computing. In a recent study conducted by NASA and Google using the "Sycamore Processor"; a task was engineered which took 200 seconds to be completed using quantum computing. The same task would take about 10,000 years to be completed using a classical supercomputer [88]. Therefore, conducting a MD simulation on such a system would take mere seconds, even if the number of particles is of the order of 10^{10}. Hence, it is easier to assess the importance and scope of research using MD that can be conducted in the future.

Chapter 3. Simulation Methodology

3.1 Simulation Details

A number of simulations were conducted in order to predict the viscosities and critical properties of heavy hydrocarbons, details of which can be found in the sections below.

All simulations were performed on computer system housing an Intel Core i7-6700 CPU and 8 GB of RAM. With the aid of the in-built boost system, the simulations were consistently run at a clock speed of 3.95 GHz instead of the base speed of 3.40 GHz. Additionally, the simulations were performed on a single core; thereby not taking advantage of the parallelization nature of MD simulations. Moreover, all simulations used a switching function for the calculations involving the intermolecular potential. The inner cutoff was set to be 9.0 Å, while the outer cutoff was 12.0 Å. The inner cutoff was set according to the values provided by the system building software, Moltemplate [89]. The outer cutoff was based on 3σ for the CH_2 group as provided by the TraPPE force-field (see Table 3). Although, it is usually taken to be 2.5σ as recommended by Smit and Toxaevard [60], [61]; the value is rounded off to provide more accurate set of results. Furthermore, in order to visualize the results of the simulations, the Open Visualization Tool (OVITO) was used. Lastly, Table 3 below depicts the Lennard-Jones parameters for the different force-fields employed:

Table 3: LJ parameters for the AMBER, COMPASS and TraPPE force-field.

Force-Field		**ε/k_B, K**	**σ, Å**
AMBER	C atom (CH_3)	55.1	3.40
	H atom (CH_3)	7.90	2.65
	C atom (CH_2)	43.3	3.40
	H atom (CH_2)	7.90	2.47
COMPASS	C atom	31.2	3.854
	H atom	11.6	2.878
TraPPE	CH_3 Group	98.0	3.75
	CH_2 Group	46.0	3.95

3.1.1 Viscosity simulations. The Green-Kubo formalism with EQMD was used to calculate the viscosity of the three hydrocarbons using the AMBER (an all-atom model) force-field. All simulations were conducted using the LAMMPS (Large-scale Atomic/Molecular Massively Parallel Simulator) module built into the MAPS (Materials and Process Simulation) by Scienomics software [90]. Moreover, all systems consisted of 150 molecules and simulations were performed with a time-step of 1 fs. Initially, the system was first equilibrated by running it for 500-700 ps using the NPT ensemble at a pressure of 1 atm and the desired temperature. After the equilibration run, the system was then simulated in the NVE ensemble for 5 ns, after which the system was analyzed for the viscosity readings.

For the same system at the desired temperature, three simulations were conducted. This is because the viscosity results from a single simulation greatly fluctuates and running the simulation again with the same conditions would provide a different result as to the one obtained before. Hence, three simulations were performed at the same conditions after which an average of the viscosity results was taken.

In order to reduce the computational time, only the very first simulation for equilibration was conducted at 700 ps in the NPT ensemble. After the calculation of viscosity from the NVE ensemble; the same system was run for 500 ps at the NPT ensemble for the next run. This allows in the reduction of the computational time, especially in the long run where a significant number of simulations were required to be performed. This method is illustrated in Figure 29 below:

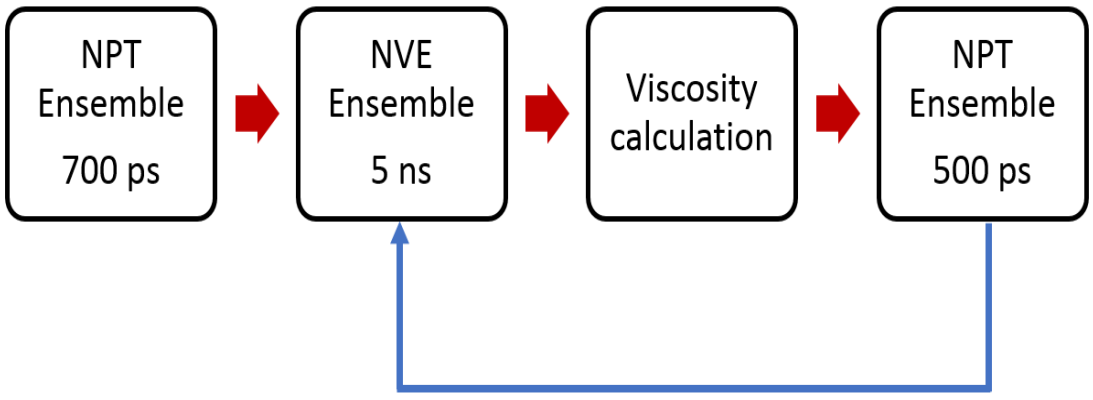

Figure 29: Schematic for carrying out viscosity simulations.

3.1.2 Critical Properties

3.1.2.1 Critical properties from molecular dynamics. In order to predict the critical properties using MD, the VEMD method was used. Furthermore, to study the effect of different potential models, three different force-fields were used to predict the critical properties of the heavy hydrocarbons. These were AMBER (all-atom model), COMPASS (all-atom model) and TraPPE (united atom model). Figure 30 below depicts n-decane molecule for the three force-fields:

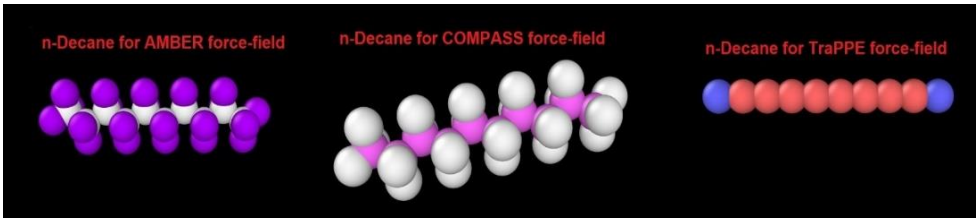

Figure 30: n-Decane as made using different force-fields

Two software packages were used to conduct the simulation. The first software used was Moltemplate [89]. This software allows the building of a molecule according to the parameters of a force-field and consequently, a box containing the desired number of molecules. Such a box is shown in Figure 31 for n-decane that was made using the TraPPE force-field. The second software used was LAMMPS [91] in order to carry out the simulations on the system that was made using Moltemplate. For all simulations, a time-step of 1 fs was employed, and the number of molecules was set to 1000 for cases below the boiling point of the hydrocarbon, and 8000 for the cases above the boiling point. This was done to ensure the formation of a stable interface at higher temperatures.

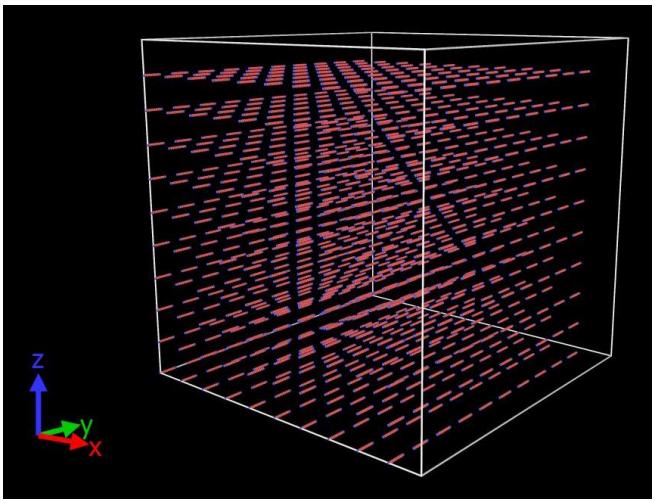

Figure 31: Initial simulation box containing 1000 n-decane molecules made with the TraPPE force-field using the Moltemplate software.

As shown in Figure 31, the box is not only very large but also contains very large spacing between the molecules. In order to produce a more realistic system, the steps as provided by Moltemplate are used as a reference [89]. The steps that are carried out are as follows:

1. Running the system for 5 ps at NVE and 50 ps at NVT ensembles at a temperature of 900 K in order to reorient the molecules and change their direction to a more natural one.
2. In order to reduce the size of the box, the system was then run in the NPT ensemble with a pressure of 250 atm for 250 ps. Additionally during this run the temperature was decreased from 900 K to the desired temperature required.
3. After the first NPT run at high pressure, a second NPT run is performed where the pressure is reduced from 250 atm to 1 atm, with the desired temperature being held constant, at 250 ps.
4. Lastly, a final NPT run is conducted at 1 atm and desired temperature for 500 ps. This run allows the system to reach a constant and realistic density at the given temperature and pressure.

Performing the above steps allows the molecules to have a more natural and realistic orientation. Moreover, it allows the system to reach an equilibrium density, as shown in Figure 32, which also shows the density of the system at different stages of the simulation.

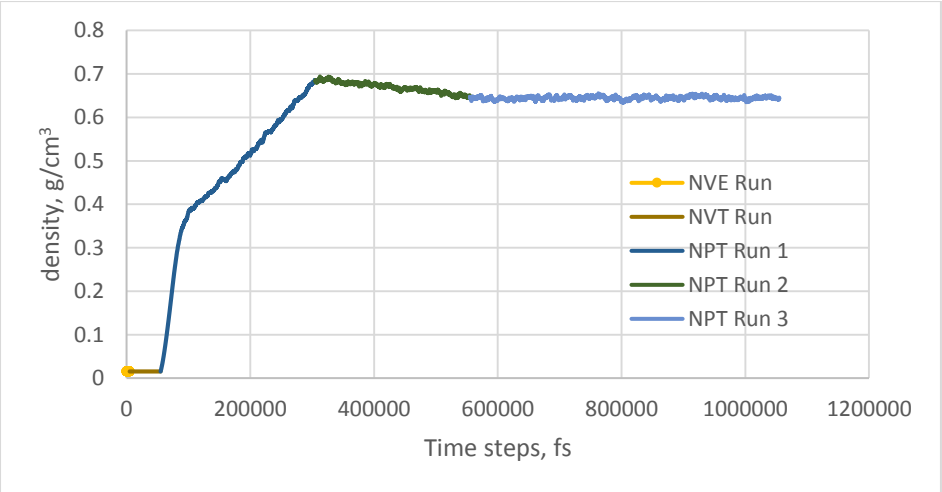

Figure 32: Density profile for n-decane during the different stages of simulation for equilibration. The desired temperature is 380 K and the force-field used is TraPPE.

After the final NPT run, the box is then suddenly enlarged in the x-dimension by using a factor of 3.5 and the system is run at the desired temperature for 0.75 ns to 3 ns. The density of the system is continuously monitored to assess if the system has reached equilibrium or not. After equilibrium has been attained, the final liquid and vapor density is recorded. Appendix A provides snapshots for the development of the density profile of a simulation for n-decane at 380 K.

3.1.2.2 Critical properties from monte-carlo. The simulations involving MC were carried out in the Towhee module of the MAPS by Scienomics software [90]. The simulations consisted of a total of 150 molecules. The simulations were performed for 1.5 million moves and using the AMBER force-field. Additionally, 6 moves were performed during the course of the simulation. The moves, along with their probability and acceptance ratios are presented in Table 4 below:

Table 4: Types and probability of moves and acceptance ratios used in predicting critical properties using MC simulation.

Type of Move	**Probability of move**	**Acceptance ratio**
Center-of-mass molecule translation move	0.833	0.5
Rotation about the Center-of-mass move	1.0	0.5
Intramolecular single atom translation move	0.667	0.5
Configuration-bias two box molecular transfer move	0.5	-
Rotational-bias two box molecular transfer move	0.333	-
Isotropic volume move	0.167	0.5

3.2 Validity of Results

In order to verify the results obtained from molecular simulations; the results were compared with various experimental data and correlations. For viscosity, a number of sources for experimental data were found and compared with the results of simulations. Table 5 below lists out the references and systems studied along with the experimental technique for measuring the viscosity of the different hydrocarbons:

Table 5: References used for viscosity experimental data of n-decane, n-pentadecane and n-eicosane.

Reference	**Systems Studied**	**Experimental Technique**
Knapstad et al. [92]	n-C6, n-C7, n-C8, n-C10, n-C12, n-C14	Absolute Oscillating Viscometer
Klein et al. [93]	n-C6, n-C8, n-C10, n-C16	Surface Light Scattering
Yucel et al. [94]	n-C12, n-C13, n-C15	Anton Paar SVM 3000 Stabinger Viscometer
Hogenboom et al. [95]	n-C12, n-C15, n-C18	Rolling-ball Viscometer
NguyenHuynh et al. [96]	Several n-alkanes, including n-C10, n-C15 and n-C20	DIPPR database
Gross & Zimmerman [97]	n-C20	N/A

The critical properties predicted from the different force-fields were compared with experimental data from Ambrose [98]. The experimental data from Ambrose lacks the critical density for n-eicosane, hence, Equation (72) was used to calculate the critical density using the experimental critical temperatures and pressures. Moreover, experimental vapor-liquid equilibria data for n-decane [99] was also used to compare

with the results of the simulations. In addition to the experimental data, results predicted by several correlations were also compared with the results obtained from the molecular simulations. Table 6 below presents the references for the employed correlations:

Table 6: Correlations used for predicting critical points employed in this work for comparison purposes.

Correlation	**Reference**
Asymptotic Behavior Correlation (ABC) by Gasem	[100]
Riazi & Sahhaf	[11]
Pakmakar-Ivan Topological Index by Vakili-Nezhaad &	[101]
Teja et al.	[102]
Tsonopoulous (1993)	[103]
Tsonopoulous (1987)	[104]
Joback's group contribution method	[105]
Lydersen's group contribution method	[106]
Klincewicz's group contribution method	[107]
Fedor's group contribution method	[108]
Ambrose's group contribution method	[109], [110]

The above correlations only provide a single point for comparison. In order to study the performance of the force-fields in predicting the vapor and liquid densities, three equation of states (EOS) were also used; namely, the Peng-Robinson (PR), Soave-Redlich-Kwong (SRK) and the Wilson's EOS. These EOS were used to provide an insight on the accuracy of the force-fields in predicting the vapor and liquid densities.

Chapter 4. Results and Discussion

4.1 Results

4.1.1 Viscosity. EQMD simulations were conducted using the MAPS by Scienomics software to study the effect of temperature on the viscosity of the liquid hydrocarbons under study in this work. Because of time limitations, only the AMBER force-field was used. Figures 33-35 depicts the results obtained from the simulations, along with the experimental results, for n-decane, n-pentadecane and n-eicosane respectively.

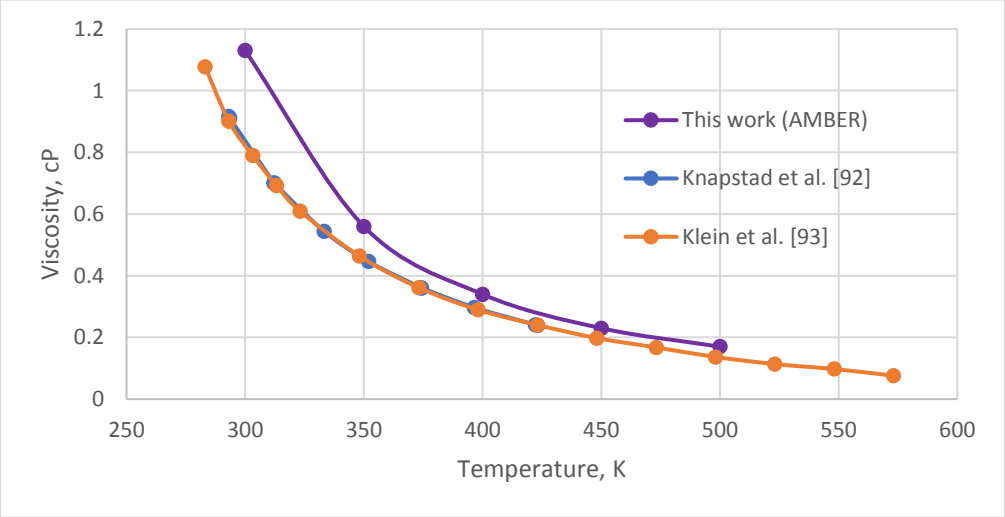

Figure 33: Viscosity for n-decane using AMBER force-field at different temperatures

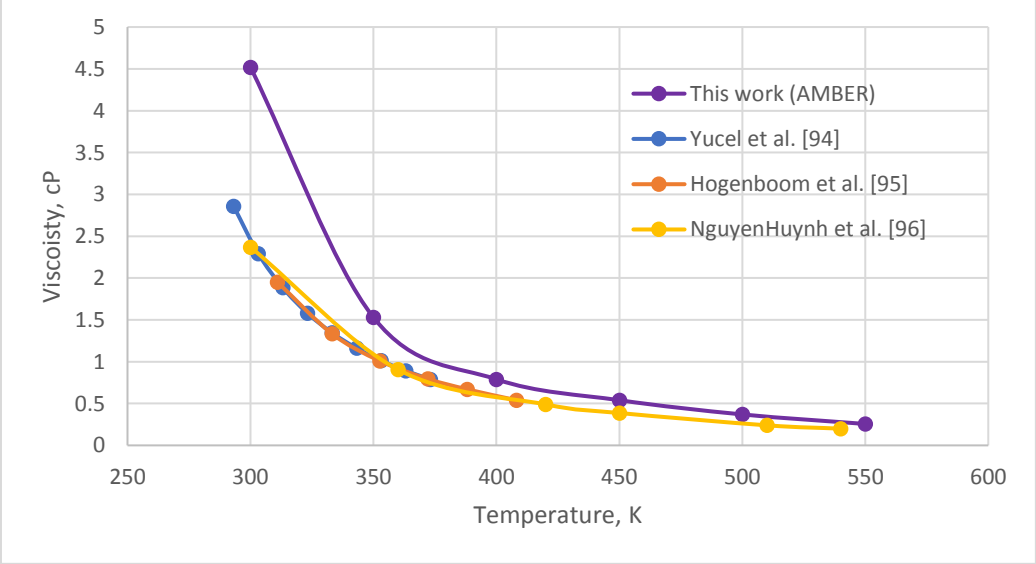

Figure 34: Viscosity for n-pentadecane using AMBER force-field at different temperatures

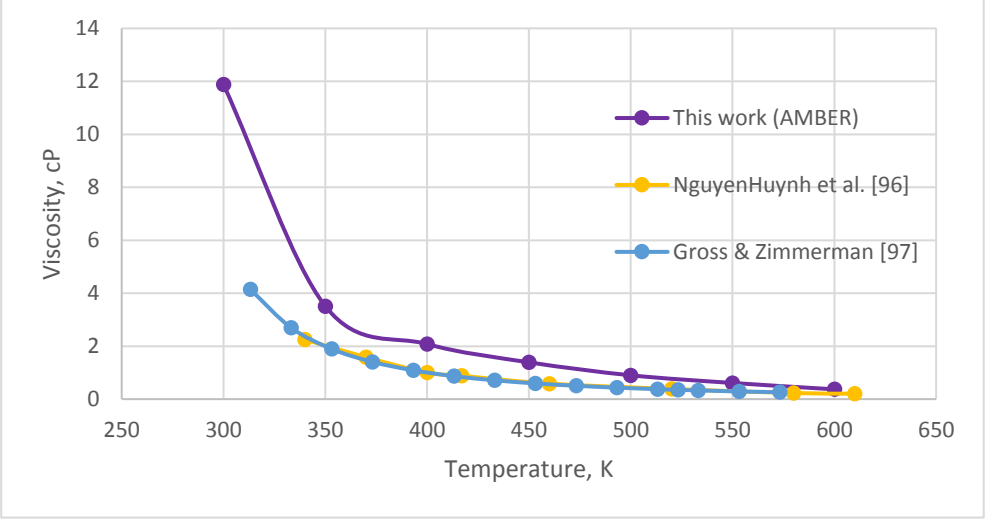

Figure 35: Viscosity for n-eicosane using AMBER force-field at different temperatures

4.1.2 Critical properties. For the critical properties, the AMBER, COMPASS and TraPPE force-fields were used. For the case of AMBER, both MD and MC simulations were conducted. Several correlations and EOS were also used for cross-comparison of the molecular simulations results.

The coexistence curves for n-decane are presented in Figure 36 for the AMBER, COMPASS and TraPPE force-fields.

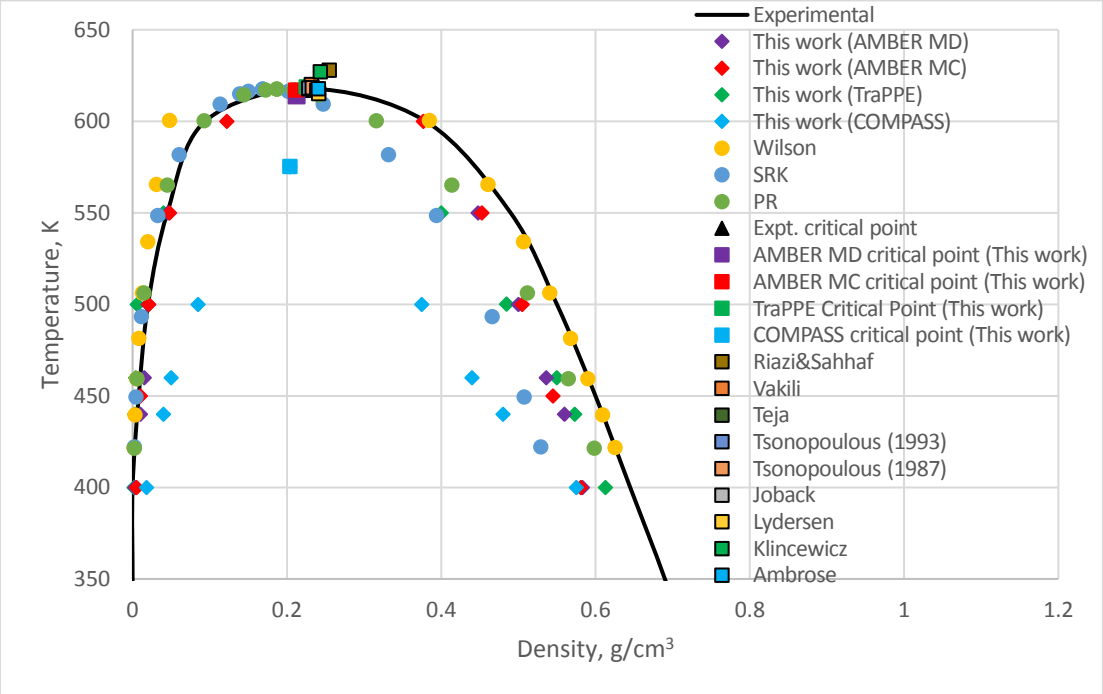

Figure 36: Coexistence curves and critical points for n-decane as predicted by the AMBER, TraPPE and COMPASS force-fields.

Figure 37 below depicts the coexistence curves obtained for n-pentadecane using the different force-fields.

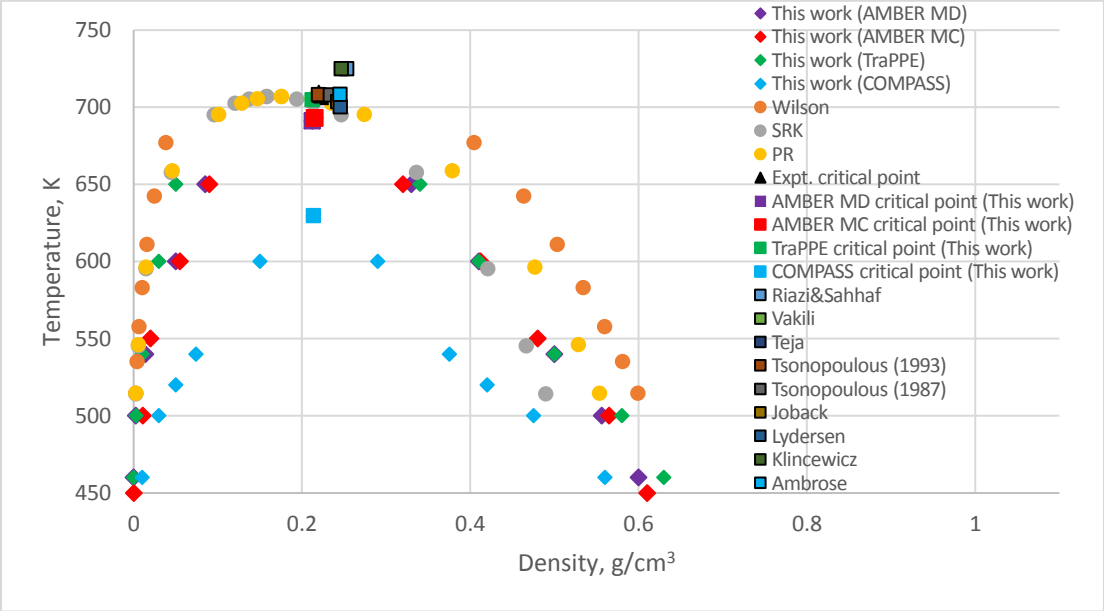

Figure 37: Coexistence curves and critical points for n-pentadecane as predicted by the AMBER, TraPPE and COMPASS force-fields.

The results for the coexistence curves of n-eicosane are presented in Figure 38 below. It is important to note that experimental data for the critical density was not found. Hence, Equation (72) is used along with the experimental critical temperature and pressure and density data from [99] to calculate the critical density.

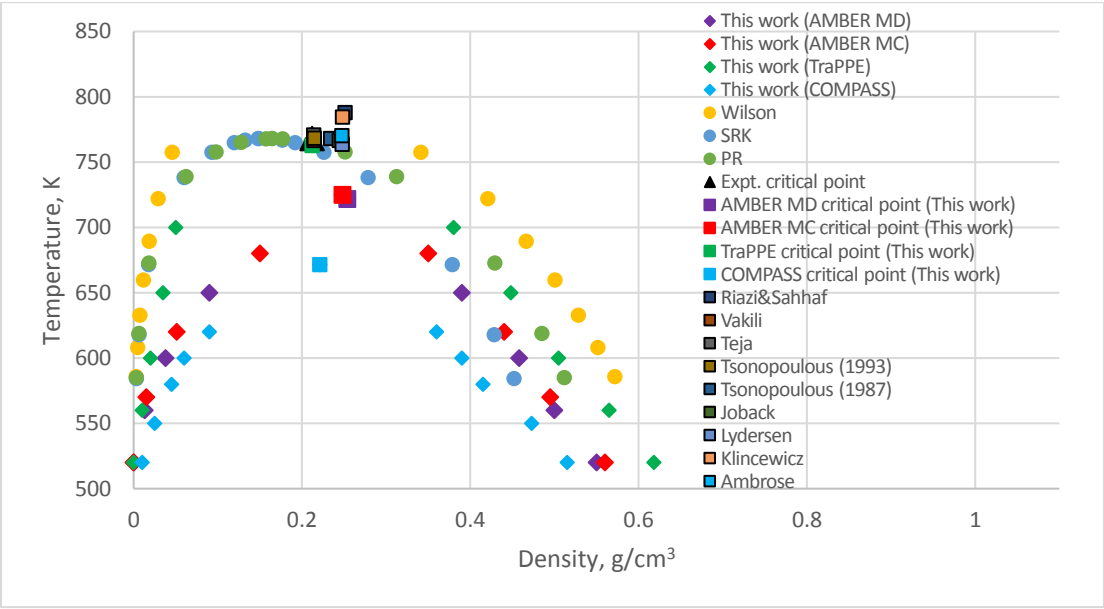

Figure 38: Coexistence curves and critical points for n-eicosane as predicted by the AMBER, TraPPE and COMPASS force-fields.

The critical pressures as obtained from the Vetere's equation (Equation (72)), as well as the experimental data, are presented in Figure 39 below.

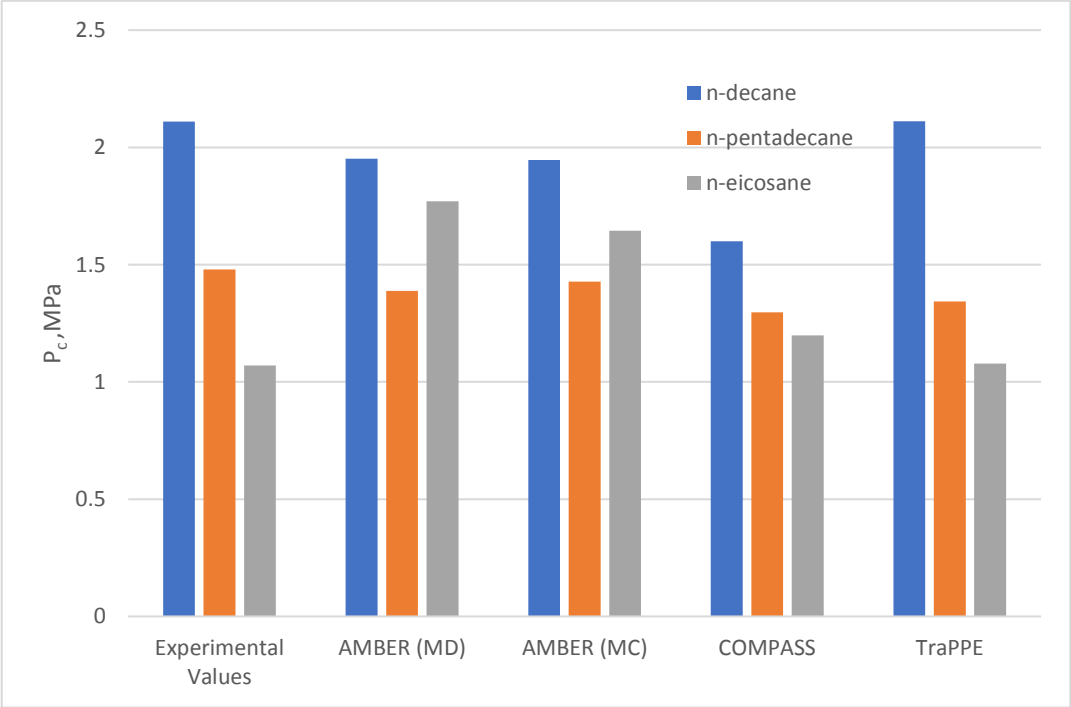

Figure 39: Critical pressure as calculated for n-decane, n-pentadecane and n-eicosane from the simulated critical temperatures and densities.

Lastly, the critical values as obtained from the simulations are presented in Tables 7 (for critical temperature), 8 (for critical density) and 9 (for critical pressure) below. The values in the square brackets represent the percentage deviation from the experimental values.

Table 7: T_c (K) for the three heavy hydrocarbons investigated as predicted by different force-fields (Values in square brackets represent the percentage deviation from the experimental data).

Hydrocarbon	**Experimental Data, K**	**AMBER (MD), K**	**AMBER (MC), K**	**COMPASS, K**	**TraPPE, K**
n-decane	617.7	614.2 [-0.57%]	617.0 [-0.11%]	575.1 [-6.89%]	618.9 [0.19%]
n-pentadecane	708.0	691.1 [-2.38%]	693.0 [-2.12%]	629.8 [-11.05%]	704.9 [-0.44%]
n-eicosane	768.0	721.7 [-6.03%]	724.9 [-5.60%]	671.5 [-12.57%]	762.7 [-0.69%]

Table 8: ρ_c (g/cm^3) for the three heavy hydrocarbons investigated as predicted by different force-fields (Values in square brackets represent the percentage deviation from the experimental data)

Hydrocarbon	Experimental Data, g/cm^3	AMBER (MD), g/cm^3	AMBER (MC), g/cm^3	COMPASS, g/cm^3	TraPPE, g/cm^3
n-decane	0.228	0.213 [-6.77%]	0.211 [-7.36%]	0.204 [-10.5%]	0.225 [-1.32%]
n-pentadecane	0.220	0.212 [-3.47%]	0.215 [-2.27%]	0.202 [-8.26%]	0.212 [-3.54%]
n-eicosane	0.212 (From Equation (72))	0.254 [19.7%]	0.248 [17.0%]	0.221 [4.31%]	0.212 [-0.02%]

Table 9: P_c (MPa) for the three heavy hydrocarbons investigated as predicted by different force-fields (Values in square brackets represent the percentage deviation from the experimental data).

Hydrocarbon	Experimental Data, MPa	AMBER (MD), MPa	AMBER (MC), MPa	COMPASS, MPa	TraPPE, MPa
n-decane	2.11	1.95 [-7.53%]	1.95 [-7.73%]	1.60 [-24.2%]	2.11 [0.07%]
n-pentadecane	1.48	1.39 [-6.20%]	1.43 [-3.49%]	1.30 [-12.4%]	1.34 [-9.22%]
n-eicosane	1.07	1.77 [65.5%]	1.64 [53.7%]	1.20 [12.0%]	1.08 [0.77%]

4.1.3 Computational efficiency. The computational efficiency takes into account the number of steps completed per day by a force-field. The measurement of the steps performed provides insight into the effectiveness of each force-field, as computational time is crucial in carrying molecular simulations that provide accurate results. Additionally, knowing the number of steps that can be computed per day allows for planning the number of simulations that can be carried out in a given period of time.

Such a comparison is provided in Figure 40 below for a system of 1000 n-decane molecules in an enlarged box (in one dimension) at 520 K. Figure 40 presents data in time steps of nanoseconds per day (ns/day) for all three force-fields: AMBER, COMPASS and TraPPE.

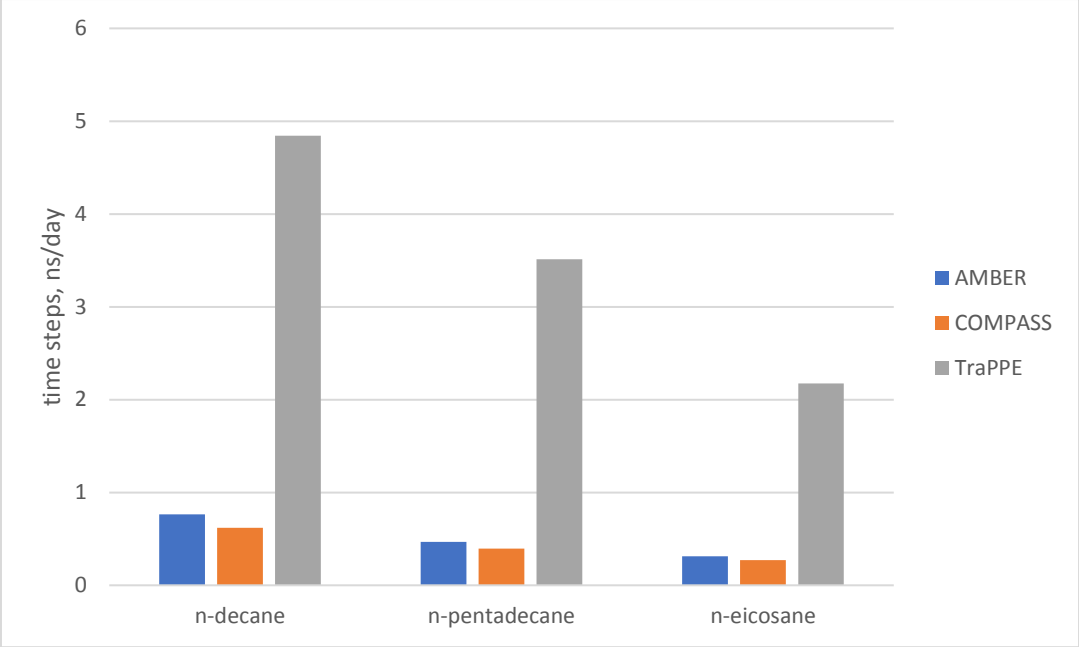

Figure 40: Time performance comparison for different force-fields for different n-alkanes in a one-dimensional box at 520 K.

4.2 Discussion

4.2.1 Viscosity. The viscosity for n-decane, n-pentadecane and n-eicosane were predicted using the AMBER force-field in EQMD. From Figures 33, 34 and 35, it can be observed that the use of AMBER force-field over-estimates the viscosity of the studied hydrocarbons for all temperatures. Additionally, it can be seen that at lower temperatures, and especially at ambient conditions, the viscosity is greatly overpredicted. For example, at 300 K for n-eicosane (Figure 35), the percentage deviation is 112% from the experimental value while at 600 K it is 76.2%. Such a trend is also observed for n-decane (Figure 33: 40.5% at 300 K and 25.0% 500 K) and n-pentadecane (Figure 34: 83.0% at 300 K and 34.7% 550 K). The reason for this trend can be attributed to the process of crystallization of the hydrocarbons at ambient temperatures; which results in poor modelling by the AMBER force-field. This is especially true for the heavier hydrocarbons, n-pentadecane and n-eicosane. Additionally, it can be seen that at 300 K, n-decane has the lowest deviation from the experimental results, followed by n-pentadecane and n-eicosane. This further proves the poor effect of crystallization or solidification process of the hydrocarbons on AMBER. Such an effect has also been observed for the OPLS force-field. In a study by Siu et al. [111], it was seen that at a temperature of 298.15 K the viscosity for n-

pentadecane was over 7000 cP as compared to the experimental value of 2.54 cP. This result is due to the formation of a "gel" or crystalline phase. Similarly, for n-decane, the OPLS force-field predicts the viscosity to be 1.386 cP (at 298.15 K), with a percentage deviation of 65%, providing similar results to the one presented in this work for n-decane using AMBER (percentage deviation of 40.5% at 300 K). However, the main objective of this study [111] was to optimize the OPLS force-field into providing better results; the result of which is the L-OPLS force-field. Using L-OPLS, the viscosity prediction at 298.15 K for n-decane and n-pentadecane turned out to be 1.102 cP (percentage deviation of 31.1%) and 3.496 cP (percentage deviation of 37.6%), respectively.

Another study conducted on n-hexadecane (n-C16) also shows similar behavior where the viscosity predicted by AMBER is extremely high as compared to the experimental data [112]. According to this study, at high temperature and high-pressure conditions, the prediction of viscosity by AMBER was found to be more accurate when compared to the experimental results. Figure 41 below represents the results obtained from that study [112]:

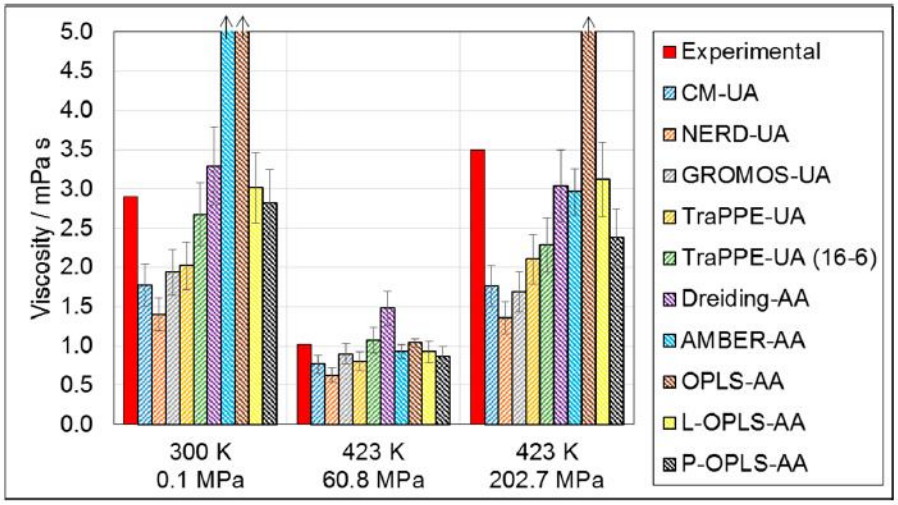

Figure 41: n-Hexadecane viscosity predictions using different force-fields compared with experimental data [112]

Lastly, a study performed on n-hexane (n-C6) showed more accurate predictions for viscosity [113]. This fits the trend that is observed in Figures 33, 34 and 35, where lighter hydrocarbons fit the AMBER force-field much better than heavier hydrocarbons. Figure 42 depicts the simulated results for n-C6 with the experimental data:

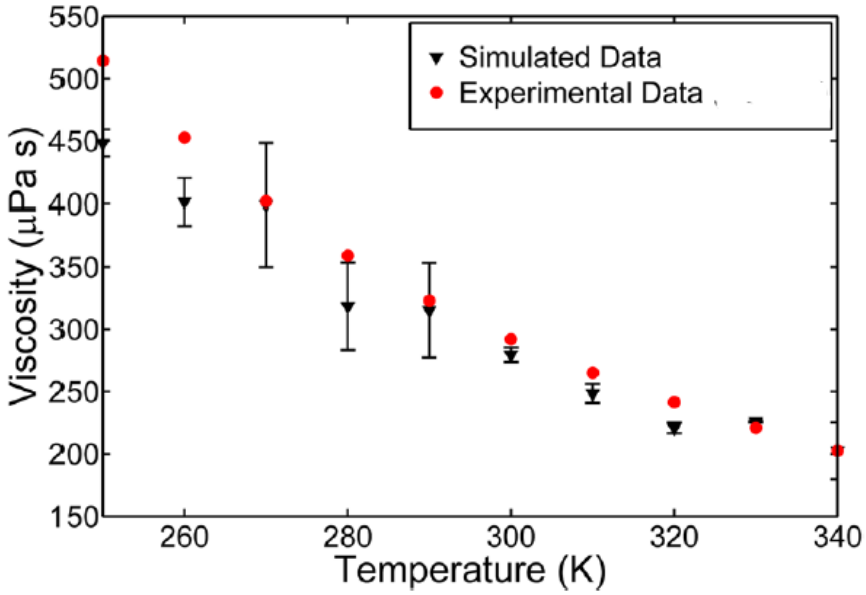

Figure 42: n-Hexane viscosity results from AMBER force-field with experimental data [113]

4.2.2 Critical properties. As stated before, for each of the three heavy hydrocarbons studied in this work (n-C10, n-C15, and n-C20), three different force-fields were used to predict the critical properties, i.e., AMBER, TraPPE, and COMPASS. The results generated by molecular simulation in this work were compared to those of several correlations, EOS and experimental data. Figures 36-48 and Tables 7-9 present the results obtained for the critical properties T_c, ρ_c, and P_c.

Referring to Tables 7-9, it can be seen that TraPPE, followed by AMBER, provide the best results in prediction of the critical properties. For TraPPE, all percentage deviations are less than 10% with the prediction of the critical temperatures being less than 1%. The AMBER force-field also provides accurate results for the critical properties. However, it can be seen that, compared to TraPPE, the percentage deviations are higher. For example, TraPPE has a percentage deviation of only -0.69% for the critical temperature of n-eicosane, while it is -6.03% and -5.60% for the AMBER MD and MC results, respectively. Furthermore, compared to AMBER and TraPPE, the COMPASS force-field provides results that are least accurate, having a percentage deviation as high as 12.57% for the critical temperature of n-eicosane. However, for the critical density, COMPASS provides a better prediction than AMBER for n-eicosane, where the percentage deviation is 4.31% for COMPASS and 19.7% and 17.0%, respectively for AMBER MD and MC. Lastly, comparing the generated results in this

work with those generated by different available correlations, it is observed in Figures 36-38 that the results from the AMBER and TraPPE force-fields fall within the range of several correlations, thus proving the accuracy and reliability of the said force-fields. For further results calculated using the correlations; Appendices B, C and D provide the numerical values of critical temperature, density and pressure respectively.

From Figure 39 and Table 9; the values of critical pressure predicted by the force-fields are compared to the experimental results. Similar to the results of critical temperature and density, the TraPPE force-field provides the most accurate results, with a maximum percentage deviation of -9.22% for n-pentadecane. Moreover, although the COMPASS force-field provides poor predictions for n-decane and n-pentadecane, it gives better accuracy in the case of n-eicosane when compared with AMBER.

In order to compare and assess the predictive capability for the molecular simulation techniques used in this study for the equilibrium (coexisting) liquid and vapor densities, results using the different the force-fields were compared with those generated by well-known EOS, i.e., Wilson, SRK and PR. In the case of n-decane, experimental vapor-liquid data were also used for comparison.

In the case of AMBER, there seems to be good agreement with the simulated results and the experimental data (and even with results from PR and SRK to some extent) for n-decane for the vapor density (see Figure 36). However, AMBER underpredicts the liquid density when compared to the experimental data. Rather, the liquid density more closely follows the trend set by PR, specifically at high temperatures. In comparison to n-decane, the vapor densities for n-pentadecane (Figure 37) and n-eicosane (Figure 38) show poor agreement for all EOS. The liquid densities for n-pentadecane and n-eicosane, on the other hand, agree well with the SRK EOS at high temperatures, similar to n-decane for PR EOS.

For the TraPPE force-field, similar trends are observed for n-decane (Figure 36) when compared to AMBER, where the vapor density follows closely the experimental data, PR and SRK data. While the liquid density from TraPPE more closely follows the liquid density predicted by PR. Additionally, for n-pentadecane (Figure 37), the vapor density is again in good agreement with the results from PR and SRK. While for the liquid density, the TraPPE predictions match closely with those by the SRK EOS.

However, for n-eicosane (Figure 38), again similar trends are seen to that of AMBER, where the vapor density is poorly predicted by TraPPE. Whereas the liquid density at high temperatures follows the trend set by PR EOS.

Lastly, the COMPASS force-field severely underpredicts both the liquid and vapor densities for all hydrocarbons and compared to AMBER and TraPPE, provides the most inaccurate results.

Considering the results obtained from molecular simulations, it is observed that the TraPPE force-field, followed by AMBER, provides the most accurate results when compared to the experimental data. They are also in the best agreement with results generated by other correlations and EOS. This may be attributed to the fact that TraPPE is designed to have specific parameters in order to predict accurate phase equilibria properties of different species (such as n-alkanes and ketones). For AMBER, a clear trend is observed where the percentage deviations seem to increase with the carbon number for all critical properties. This trend has also been observed for the viscosity results. Hence, the increase in percentage deviation could be attributed to the increase of crystallization in the system which AMBER is unable to quantify accurately. This fact is further proved by the accurate prediction (when compared to EOS) of liquid viscosities at higher temperatures.

In this work, the least accurate of the three employed force-fields has been COMPASS, with inaccurate results obtained for critical properties and liquid and vapor densities. This could be attributed to the fact that COMPASS does not place equal emphasis between intramolecular and intermolecular parameters. Similar results have also been produced in another study in the literature, for different hydrocarbons simulated with different force-fields [114], including AMBER, TraPPE and COMPASS, where the most accurate results were produced by TraPPE followed by AMBER and COMPASS, as it is the case in this work. It was also observed in that study, that for smaller molecules, AMBER predicts the vapor density much more accurately with a greater set of results showing a deviation of only 1%, which is similar to the trends observed in this work where AMBER produces the vapor density for n-decane similar to the experimental data. In a different study [115], it was also observed that the TraPPE force-field predicts liquid densities that are in good agreement with the

Lemmon and Huber EOS for n-dodecane. These results are similar to the results obtained in this work for other hydrocarbons.

Apart from the critical properties obtained from MD, results from the MC simulations using AMBER were also provided. In theory, it is expected that any result from MC and MD should be the same. From the results obtained, it can be clearly seen that MC and MD do provide similar results. Small differences in the final results arise from the minor fluctuations that take place during the course of the simulations and also because of significant figures.

It is also important to note here that the results for critical pressure were obtained from the simulated results of critical temperature and critical density by means of Equation (72). Because of this, the errors for critical pressure are much higher, as the small errors and inaccuracy in critical temperatures and density are greatly amplified.

4.2.3 Computational efficiency. An important aspect of molecular simulations is the execution time required for carrying out these simulations. In an effort to reduce the computational time, different force-fields were developed (such as the united-atom TraPPE force-field) that simplify the intermolecular calculations, thereby reducing the computational time. Hence, it becomes of value to provide a comparison between the computational time for the different force-fields used in this study in order to gauge the computational efficiency. However, this aspect must be looked while taking into account the accuracy of the generated simulation results.

The computational time greatly depends on the models used and also, on the number of particles in the system. In this work, two different models were used to design the three force-fields that were used in this study. The first model is the All-Atom model (AA), which was used for the AMBER and COMPASS force fields, while the second is the United-Atom model (UA) for the TraPPE force-field. The results for the time performance are shown in Figure 40.

From Figure 40, two trends are observed: 1) for all hydrocarbons, the TraPPE force-field provides the highest number of time-steps computed followed by AMBER and COMPASS, and 2) with the increase in the carbon number, the number of time-steps for all force-fields tends to decrease. These trends can be attributed to the AA and UA nature of the force-fields. In the AA model, all atoms are modelled, which in the

case of n-alkane would include hydrogen and carbon atoms. UA model, on the other side, only looks at a group of atoms. For example, for n-alkanes, there will be two methyl groups, while the rest will be the methylene groups. This greatly reduces the number of interaction sites for a UA model when compared to AA model, leading to better computational performance.

Based on the results obtained for critical properties and those presented in Figure 40; it can be concluded that TraPPE provides with the most accurate results while being efficient in terms of the computational time required.

Finally, it is necessary to state that the simulations were not carried in a parallel system. Parallelization is an important aspect of MD simulations and computational methods in general, where a task is broken into chunks and a number of cores on a CPU or multiple CPUs are utilized to reduce the computational time. In this work, the computer system would utilize a maximum of 15% of its speed by using a single core. The use of a single core ensures that the CPU is adequately cooled using stock cooling apparatus. Hence, in order to increase the number of cores used, and thereby reduce the computational time, a system would require more efficient form of cooling. Figure 43 below shows this percent utilization:

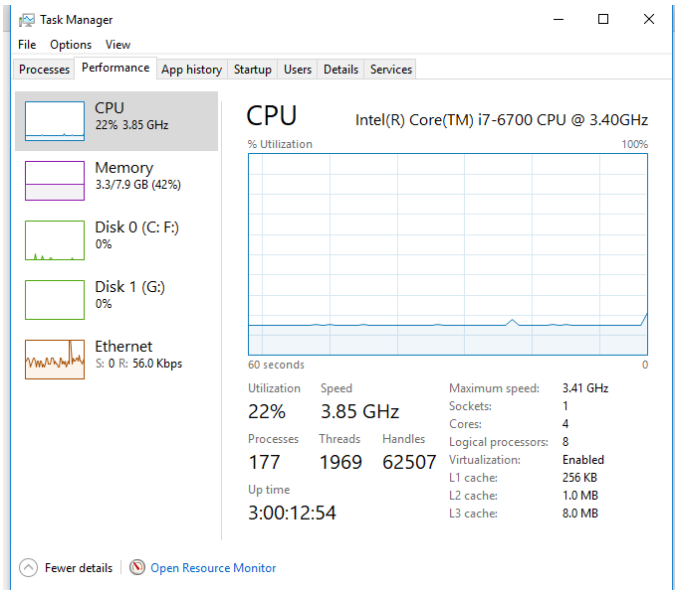

Figure 43: Percent utilization of the CPU. Note: the spike in utilization is due to the command for screenshot. Steady state value is at 15%.

Hence, it can be concluded that increasing the utilization of the number of cores on this system would greatly increase the computational efficiency.

Chapter 5. Conclusion and Recommendations

The aim of this thesis is to use molecular simulation to predict the viscosity and critical properties of the heavy hydrocarbons n-decane, n-pentadecane and n-eicosane. This was primarily done using MD. The following sections provide the key conclusions and further recommendations coming out of this work.

5.1 Viscosity Study

Through the use of EQMD with Green-Kubo relations, the viscosity of n-decane, n-pentadecane and n-eicosane were studied for the first time using the AMBER force-field as a function of temperature. It was observed that AMBER poorly models the viscous behavior of heavier molecules at lower temperatures. This is especially true at ambient temperature, where the percentage deviation for n-pentadecane and n-eicosane are found to reach 83 and 112%. From these it can be concluded that AMBER is unable to accurately model such heavy species.

It is recommended to use other force-fields in predicting the viscosities of heavy hydrocarbons and establish as to which force-field provides greater accuracy. Also, to further illustrate the possible effects of crystallization, the AMBER force-field can be used to study the viscosities of lighter hydrocarbons. This will further help to verify the trends that were observed in the thesis. The viscosity of mixtures of heavy hydrocarbons can also be studied using molecular simulation whereby the hydrocarbon system can be modelled similar to an actual heavy oil system.

5.2 Critical Properties Study

The primary method of predicting the critical properties of heavy hydrocarbons, or any species in general, is through the use of Gibbs ensemble Monte Carlo. However, a major disadvantage of using MC techniques is the lack of parallelization on a computational system which leads to increasing computational time. Hence, the use of MD to predict critical properties is being extensively researched.

In this thesis, MD simulations, specifically VEMD, were used to predict the critical properties of n-decane, n-pentadecane and n-eicosane, using the AMBER, COMPASS and TraPPE force-fields. Although n-decane and n-eicosane critical

properties have been investigated using the TraPPE force-field [33], n-pentadecane is studied in this work for the first time using AMBER, COMPASS and TraPPE. Additionally, no studies were found in open literature on the prediction of critical properties for n-decane and n-eicosane using AMBER and COMPASS force fields.

From the results generated in this work, it can clearly be seen that TraPPE is the most accurate force among the three fields studied for predicting the critical properties with maximum percentage deviation of -9.22%. The second most accurate force-field is AMBER followed by COMPASS. Moreover, when compared to other correlations, it is observed that TraPPE fits well within the results of most correlations.

Additionally, when compared with EOS, it is observed that when the carbon number of the hydrocarbons increases (i.e., for heavier hydrocarbons), the liquid density predicted by TraPPE and AMBER were in good agreement with those predicted by EOS. For n-decane, both TraPPE and AMBER provide good agreement with the experiment vapor density as well. However, this is not the case for COMPASS force field for all species where it generated the worst prediction for vapor and liquid densities.

Based on the findings in this study, it is recommended to use TraPPE and AMBER, and other force-fields, such as CHARMM, to predict and study the critical properties of heavier hydrocarbons. Additionally, it is also important to study mixtures of heavy hydrocarbons. Hence, it is recommended to find a model heavy hydrocarbon system that can be used with different force-fields in order to study the critical properties of such a mixture.

5.3 Computational Efficiency

The number of time steps performed by each force-field was also computed and compared. The results showed that TraPPE can compute a significantly higher number of steps because of its UA nature; followed by AMBER and COMPASS. Therefore, it can be concluded that TraPPE has the highest efficiency, since it provides with the lowest percentage deviations in critical properties while computing the highest number of time steps.

Since the critical properties with MD require a greater number of molecules, it is recommended to use parallel computer systems to greatly reduce the computational time and to make the process of predicting critical properties using MD more efficient. This can be easily implemented in a high-performance computing facility.

References

[1] F. J. Hein, "Geology of bitumen and heavy oil: An overview," *J. Pet. Sci. Eng.*, vol. 154, pp. 551–563, June 2017.

[2] R. G. Santos, W. Loh, A. C. Bannwart, O. V. Trevisan, "An overview of heavy oil properties and its recovery and transportation methods," *Brazilian Journal of Chemical Engineering*, vol. 31, no. 03, pp. 571–590, 2014.

[3] J. H. Zhang *et al.*, "Crude-oil hydrocarbon composition characteristics and oil viscosity prediction in the northern Songliao Basin," *Sci. China Earth Sci.*, vol. 57, no. 2, pp. 297–312, 2014.

[4] M. R. Gray, *Upgrading Oilsands Bitumen and Heavy Oil*. Edmonton, Canada: The University of Alberta Press, 2015.

[5] X. Dong, H. Liu, Z. Chen, K. Wu, N. Lu, and Q. Zhang, "Enhanced oil recovery techniques for heavy oil and oilsands reservoirs after steam injection," *Appl. Energy*, vol. 239, pp. 1190–1211, Apr. 2019.

[6] A. N. Sawarkar, "Cavitation induced upgrading of heavy oil and bottom-of-the-barrel: A review," *Ultrason. Sonochem.*, vol. 58, Nov. 2019.

[7] F. J. Hein, "Heavy oil and oil (tar) sands in North America: An overview & summary of contributions," *Nat. Resour. Res.*, vol. 15, no. 2, pp. 67–84, 2006.

[8] D. K. Banerjee, *Oil Sands, Heavy Oil & Bitumen : From Recovery to Refinery*. Tulsa, Oklahoma: PennWell Corp., 2012.

[9] G. M. Crawley, *Fossil Fuels : Current Status and Future Directions*. New Jersey: World Scientific, 2016.

[10] H. Lipeng, D. Bin, P. Baoliang, L. Jianhui, G. Xiangfei, and W. Pingmei, "Structure simulation and validation of Venezuela ultra heavy oil fractions," *J. Pet. Sci. Eng.*, vol. 146, pp. 1173–1178, Oct. 2016.

[11] M. R. Riazi and T. A. Al-Sahhaf, "Physical properties of heavy petroleum fractions and crude oils," *Fluid Phase Equilib.*, vol. 117, no. 1–2, pp. 217–224, 1996.

[12] W. Gao, R. L. Robinson, and K. A. M. Gasem, "Improved correlations for heavy n-paraffin physical properties," *Fluid Phase Equilib.*, vol. 179, no. 1–2, pp. 207–216, 2001.

[13] Z. Jianzhong, Z. Biao, Z. Suoqi, W. Renan, and Y. Guanghua, "Simplified prediction of critical properties of nonpolar compounds, petroleum, and coal liquid fractions," *Ind. Eng. Chem. Res.*, vol. 37, no. 5, pp. 2059–2060, 1998.

[14] G. Raabe, *Molecular Simulation Studies on Thermophysical Properties : With Application to Working Fluids*. Singapore: Springer Nature Singapore Pte Limited, 2017.

[15] M. P. Allen and D. J. Tildesley, *Computer Simulation of Liquids*, 2nd ed. Oxford: Oxford University Press, 2017.

[16] S. I. Sandler, *An Introduction to Applied Statistical Thermodynamics*. Hoboken, NJ: Wiley, 2011.

[17] R. Bowley and M. Sánchez, *Introductory Statistical Mechanics*. Oxford: Clarendon Press, 1996.

[18] D. A. McQuarrie, *Statistical Mechanics*. Sausalito, California: University Science Books, 2000.

[19] C. E. Hecht, *Statistical Thermodynamics and Kinetic Theory*, Dover ed. Mineola, N.Y.: Dover Publications, 1998.

[20] T. L. Hill, *An Introduction to Statistical Thermodynamics*. New York: Dover Publications, 1986.
[21] A. Hinchliffe, *Molecular Modelling for Beginners*. Chichester, West Sussex, England: Wiley, 2003.
[22] P. Ungerer, C. Nieto-Draghi, B. Rousseau, G. Ahunbay, and V. Lachet, "Molecular simulation of the thermophysical properties of fluids: From understanding toward quantitative predictions," *J. Mol. Liq.*, vol. 134, no. 1-3, pp. 71–89, 2007.
[23] I. W. Kuo, C. J. Mundy, M. J. McGrath, and J. I. Siepmann, "Time-Dependent Properties of Liquid Water: A Comparison of Car-Parrinello and Born-Oppenheimer Molecular Dynamics Simulations," *J. Chem. theory Comput.*, vol. 2, no. 5, pp. 1274–1281, 2006.
[24] A. Striolo, "The mechanism of water diffusion in narrow carbon nanotubes," *Nano Lett.*, vol. 6, no. 4, pp. 633–639, 2006.
[25] Y. Fomin, E. N. Tsiok, V. N. Ryzhov, and V. V Brazhkin, "Anomalous behavior of dispersion curves in water-like systems and water," *Fluid Phase Equilibria*, vol. 498, pp. 45–50, Oct. 2019.
[26] N. D. Kondratyuk and V. V. Pisarev, "Calculation of viscosities of branched alkanes from 0.1 to 1000 MPa by molecular dynamics methods using COMPASS force field," *Fluid Phase Equilibria*, vol. 498, pp. 151–159, Oct. 2019.
[27] P. Vashishta, R. K. Kalia, and A. Nakano, "Multimillion atom simulations of dynamics of oxidation of an aluminum nanoparticle and nanoindentation on ceramics," *J. Phys. Chem. B*, vol. 110, no. 8, pp. 3727–3733, 2006.
[28] H. Gould and J. Tobochnik, *An Introduction to Computer Simulation Methods : Applications to Physical Systems*, 2nd ed. Reading, Massachusetts: Addison-Wesley, 1996.
[29] D. Frenkel and B. T. Smit, *Understanding Molecular Simulation : From Algorithms to Applications*. San Diego, California: Academic Press, 2002.
[30] N. Sobecki, C. Nieto-Draghi, A. Di Lella, and D. Y. Ding, "Phase behavior of hydrocarbons in nano-pores," *Fluid Phase Equilibria*, vol. 497, pp. 104–121, Oct. 2019.
[31] I. L. G. Pereira *et al.*, "DFT and canonical ensemble investigations of gasoline additives at the gas phase: ETBE, MTBE, DIPE, ethanol and methanol," *Theor. Chem. Accounts Theory, Comput. Model.*, vol. 137, no. 10, pp. 1–10, 2018.
[32] L. Song, Z. L. Sun, and L. V. C. Rees, "Experimental and molecular simulation studies of adsorption and diffusion of cyclic hydrocarbons in silicalite-1," *Microporous Mesoporous Mater.*, vol. 55, no. 1, pp. 31–49, 2002.
[33] E. A. Müller and A. Mejía, "Comparison of united-atom potentials for the simulation of vapor-liquid equilibria and interfacial properties of long-chain n-alkanes up to n-C100," *J. Phys. Chem. B*, vol. 115, no. 44, pp. 12822–12834, 2011.
[34] R. A. Messerly, T. A. Knotts, R. L. Rowley, and W. V. Wilding, "An improved approach for predicting the critical constants of large molecules with Gibbs Ensemble Monte Carlo simulation," *Fluid Phase Equilib.*, vol. 425, pp. 432–442, Oct. 2016.
[35] J. T. Fern, D. J. Keffer, and W. V. Steele, "Measuring coexisting densities from a two-phase molecular dynamics simulation by voronoi tessellations," *J. Phys. Chem. B*, vol. 111, no. 13, pp. 3469–3475, 2007.

[36] L. D. Gelb and E. A. Müller, “Location of phase equilibria by temperature-quench molecular dynamics simulations,” *Fluid Phase Equilib.*, vol. 203, no. 1–2, pp. 1–14, 2002.
[37] M. G. Ahunbay, S. Kranias, V. Lachet, and P. Ungerer, “Prediction of thermodynamic properties of heavy hydrocarbons by Monte Carlo simulation,” *Fluid Phase Equilib.*, vol. 228–229, pp. 311–319, Feb. 2005.
[38] J. J. Potoff and J. I. Siepmann, “Vapor-liquid equilibria of mixtures containing alkanes, carbon dioxide, and nitrogen,” *AIChE J.*, vol. 47, no. 7, pp. 1676–1682, 2001.
[39] T. Ikeda, “First principles isothermal-isobaric centroid molecular dynamics simulation of high pressure ices,” *Chem. Phys. Lett.*, vol. 717, pp. 141–146, Feb. 2019.
[40] P. E. Brumby, D. Yuhara, D. T. Wu, A. K. Sum, and K. Yasuoka, “Cage occupancy of methane hydrates from Gibbs ensemble Monte Carlo simulations,” *Fluid Phase Equilibria*, vol. 413, pp. 242–248, Apr. 2016.
[41] P. Bai and J. I. Siepmann, “Gibbs ensemble Monte Carlo simulations for the liquid-liquid phase equilibria of dipropylene glycol dimethyl ether and water: A preliminary report,” *Fluid Phase Equilibria*, vol. 310, no. 1, pp. 11–18, 2011.
[42] M. Soroush Barhaghi and J. J. Potoff, “Prediction of phase equilibria and Gibbs free energies of transfer using molecular exchange Monte Carlo in the Gibbs ensemble,” *Fluid Phase Equilibria*, vol. 486, pp. 106–118, May 2019.
[43] C. L. Diel and V. F. Cabral, “Equilibrium properties of protic ionic liquids based on metil-2-hydroxyethylammonium cation,” *J. Mol. Liq.*, vol. 282, pp. 226–234, May 2019.
[44] B. M. Marwa, S. Bruno, B. Mongi, F. T. Van, and B. L. Abdelmottaleb, “Modeling of adsorption isotherms of dye N719 on titanium oxide using the grand canonical ensemble in statistical physics for dye sensitized solar cells,” *Sol. Energy*, vol. 135, p. 177, Oct. 2016.
[45] S. Wjihi, A. Erto, S. Knani, and A. Ben Lamine, “Investigation of adsorption process of benzene and toluene on activated carbon by means of grand canonical ensemble,” *J. Mol. Liq.*, vol. 238, pp. 402–410, July 2017.
[46] B. Mohamed, Z. Qingyu, G. D. Moggridge, and B. L. Abdelmottaleb, “New insight in adsorption of pyridine on the two modified adsorbents types MN200 and MN500 by means of grand canonical ensemble,” *J. Mol. Liq.*, vol. 263, pp. 413–421, Aug. 2018.
[47] P. G. M. Mileo, C. L. Cavalcante, J. Möllmer, M. Lange, J. Hofmann, and S. M. P. Lucena, “Molecular simulation of natural gas storage in Cu-BTC metal-organic framework,” *Colloids Surfaces A Physicochem. Eng. Asp.*, vol. 462, pp. 194–201, Nov. 2014.
[48] R. P. P. L. Ribeiro, B. C. R. Camacho, A. Lyubchyk, I. A. A. C. Esteves, F. J. A. L. Cruz, and J. P. B. Mota, “Experimental and computational study of ethane and ethylene adsorption in the MIL-53(Al) metal organic framework,” *Microporous Mesoporous Mater.*, vol. 230, pp. 154–165, Aug. 2016.
[49] A. Nakhli, M. Bergaoui, M. Khalfaoui, J. Möllmer, A. Möller, and A. Ben Lamine, “Modeling of high pressure adsorption isotherm using statistical physics approach: lateral interaction of gases adsorption onto metal-organic framework HKUST-1,” *Adsorpt. J. Int. Adsorpt. Soc.*, vol. 20, no. 8, pp. 987–997, 2014.
[50] C. V. D. R. Anderson and K. K. Tamma, “An overview of advances in heat

conduction models and approaches for prediction of thermal conductivity in thin dielectric films," *Int. J. Numer. Methods Heat Fluid Flow*, vol. 14, no. 1, pp. 12–65, 2004.

[51] A. D. Mackerell Jr., "Empirical force fields for biological macromolecules: Overview and issues," *J. Comput. Chem.*, vol. 25, no. 13, pp. 1584–1604, 2004.

[52] J. C. Pàmies, C. McCabe, P. T. Cummings, and L. F. Vega, "Coexistence Densities of Methane and Propane by Canonical Molecular Dynamics and Gibbs Ensemble Monte Carlo Simulations," *Mol. Simul.*, vol. 29, no. 6–7, pp. 463–470, 2003.

[53] W. D. Cornell *et al.*, "A Second Generation Force Field for the Simulation of Proteins, Nucleic Acids, and Organic Molecules," *J. Am. Chem. Soc.*, vol. 117, no. 19, pp. 5179–5197, May 1995.

[54] H. Sun, "COMPASS: An ab Initio Force-Field Optimized for Condensed-Phase ApplicationsOverview with Details on Alkane and Benzene Compounds," *J. Phys. Chem. B*, vol. 102, no. 38, pp. 7338–7364, Sept. 1998.

[55] M. G. Martin and J. I. Siepmann, "Transferable Potentials for Phase Equilibria. 1. United-Atom Description of n-Alkanes," *J. Phys. Chem. B*, vol. 102, no. 14, pp. 2569–2577, Apr. 1998.

[56] W. L. Jorgensen, D. S. Maxwell, and J. Tirado-Rives, "Development and Testing of the OPLS All-Atom Force Field on Conformational Energetics and Properties of Organic Liquids," *J. Am. Chem. Soc.*, vol. 118, no. 45, pp. 11225–11236, Nov. 1996.

[57] W. Damm, A. Frontera, J. Tirado–Rives, and W. L. Jorgensen, "OPLS all-atom force field for carbohydrates," *J. Comput. Chem.*, vol. 18, no. 16, pp. 1955–1970, Dec. 1997.

[58] A. C. T. van Duin, S. Dasgupta, F. Lorant, and W. A. Goddard, "ReaxFF: A Reactive Force Field for Hydrocarbons," *J. Phys. Chem. A*, vol. 105, no. 41, pp. 9396–9409, Oct. 2001.

[59] A. D. MacKerell *et al.*, "All-Atom Empirical Potential for Molecular Modeling and Dynamics Studies of Proteins," *J. Phys. Chem. B*, vol. 102, no. 18, pp. 3586–3616, Apr. 1998.

[60] B. Smit, "Phase diagrams of Lennard-Jones fluids," *J. Chem. Phys.*, vol. 96, no. 11, pp. 8639-8640, 1992.

[61] S. Toxværd and J. C. Dyre, "Shifted forces in molecular dynamics," *J. Chem. Phys.*, vol. 134, no. 8, 2011.

[62] C. Desgranges, K. N. Ngale, and J. Delhommelle, "Prediction of critical properties for Naphthacene, Triphenylene and Chrysene by Wang-Landau simulations," *Fluid Phase Equilib.*, vol. 322–323, pp. 92–96, May 2012.

[63] P. J. Steinbach and B. R. Brooks, "New spherical-cutoff methods for long-range forces in macromolecular simulation," *J. Comput. Chem.*, vol. 15, no. 7, pp. 667–683, 1994.

[64] N. T. Thomopoulos, *Essentials of Monte Carlo Simulation : Statistical Methods for Building Simulation Models*. New York: Springer, 2013.

[65] J. I. Siepmann, S. Karaborni, and B. Smit, "Simulating the critical behaviour of complex fluids," *Nature*, vol. 365, no. 6444, pp. 330–332, 1993.

[66] M. D. Macedonia and E. J. Maginn, "Impact of confinement on zeolite cracking selectivity via Monte Carlo integration," *AIChE J.*, vol. 46, no. 12, pp. 2504–2517, 2000.

[67] E. Bourasseau, P. Ungerer, and A. Boutin, "Prediction of Equilibrium Properties

of Cyclic Alkanes by Monte Carlo Simulation - New Anisotropic United Atoms Intermolecular Potential - New Transfer Bias Method," *J. Phys. Chem. B*, vol. 106, no. 21, pp. 5483–5491, 2002.

[68] M. N. Rosenbluth and A. W. Rosenbluth, "Monte Carlo Calculation of the Average Extension of Molecular Chains," *J. Chem. Phys.*, vol. 23, no. 2, pp. 356–359, Feb. 1955.

[69] F. Jabbari, A. Rajabpour, and S. Saedodin, "Thermal conductivity and viscosity of nanofluids: A review of recent molecular dynamics studies," *Chem. Eng. Sci.*, vol. 174, pp. 67–81, Dec. 2017.

[70] H. C. Andersen, "Molecular dynamics simulations at constant pressure and/or temperature," *J. Chem. Phys.*, vol. 72, no. 4, pp. 2384–2393, Feb. 1980.

[71] H. J. C. Berendsen, J. P. M. Postma, W. F. van Gunsteren, A. DiNola, and J. R. Haak, "Molecular dynamics with coupling to an external bath," *J. Chem. Phys.*, vol. 81, no. 8, pp. 3684–3690, Oct. 1984.

[72] J. Rivera, "Transport properties of nitrogen and n-alkane binary mixtures," *Fluid Phase Equilib.*, vol. 185, no. 1–2, pp. 389–396, 2001.

[73] B. Rousseau and J. Petravic, "Transport Coefficients of Xylene Isomers," *J. Phys. Chem. B*, vol. 106, no. 50, pp. 13010–13017, Dec. 2002.

[74] F. J. Cherne III and P. A. Deymier, "Calculation of the transport properties of liquid aluminum with equilibrium and non-equilibrium molecular dynamics," *Scr. Mater.*, vol. 45, no. 8, pp. 985–991, 2001.

[75] T. Koishi, Y. Shirakawa, and S. Tamaki, "Shear viscosity of liquid metals obtained by non-equilibrium molecular dynamics," *J. Non. Cryst. Solids*, vol. 205–207, no. 1, pp. 383–387, Oct. 1996.

[76] A. P. Markesteijn, R. Hartkamp, S. Luding, and J. Westerweel, "A comparison of the value of viscosity for several water models using Poiseuille flow in a nano-channel," *J. Chem. Phys.*, vol. 136, no. 13, p. 134104, Apr. 2012.

[77] P. Bordat and F. Müller-Plathe, "The shear viscosity of molecular fluids: A calculation by reverse nonequilibrium molecular dynamics," *J. Chem. Physics*, vol. 116, pp. 3362-3369, Feb. 2002.

[78] F. Müller-Plathe, "Reversing the perturbation in nonequilibrium molecular dynamics: An easy way to calculate the shear viscosity of fluids," *Phys. Rev. E*, vol. 59, no. 5, pp. 4894–4898, May 1999.

[79] J. J. De Pablo, "Simulation of phase equilibria for chain molecules," *Fluid Phase Equilib.*, vol. 104, pp. 195–206, Mar. 1995.

[80] F. M. S. S. Fernandes and R. P. S. Fartaria, "Gibbs ensemble Monte Carlo," *Am. J. Phys.*, vol. 83, no. 9, p. 809, 2015.

[81] N. B. Wilding, "Critical-point and coexistence-curve properties of the Lennard-Jones fluid: A finite-size scaling study," *Phys. Rev. E*, vol. 52, no. 1, pp. 602–611, July 1995.

[82] P. Virnau, M. Müller, L. G. MacDowell, and K. Binder, "Phase diagrams of hexadecane-CO 2 mixtures from histogram-reweighting Monte Carlo," *Comput. Phys. Commun.*, vol. 147, no. 1, pp. 378–381, 2002.

[83] G. C. Boulougouris, L. D. Peristeras, I. G. Economou, and D. N. Theodorou, "Predicting fluid phase equilibrium via histogram reweighting with Gibbs ensemble Monte Carlo simulations," *J. Supercrit. Fluids*, vol. 55, no. 2, pp. 503–509, 2010.

[84] D. A. Kofke, "Direct evaluation of phase coexistence by molecular simulation via integration along the saturation line," *J. Chem. Phys.*, vol. 98, no. 5, pp.

4149–4162, Mar. 1993.
[85] T. E. Gartner, T. H. Epps, and A. Jayaraman, “Leveraging Gibbs Ensemble Molecular Dynamics and Hybrid Monte Carlo/Molecular Dynamics for Efficient Study of Phase Equilibria,” *J. Chem. Theory Comput.*, vol. 12, no. 11, pp. 5501–5510, 2016.
[86] J. A. Anderson, E. Jankowski, T. L. Grubb, M. Engel, and S. C. Glotzer, “Massively parallel Monte Carlo for many-particle simulations on GPUs,” *J. Comput. Phys.*, vol. 254, pp. 27–38, Dec. 2013.
[87] B. Barney, *Introduction to Parallel Computing*, Lawrence Livermore National Laboratory, 2019. Accessed on: Nov. 28, 2019. [Online]. Available: https://computing.llnl.gov/tutorials/parallel_comp/
[88] F. Arute *et al.*, “Quantum supremacy using a programmable superconducting processor,” *Nat. Int. Wkly. J. Sci.*, vol. 574, no. 7779, pp. 505–510, 2019.
[89] A. Jewett, Z. Zhuang, and J. Shea, “Moltemplate a Coarse-Grained Model Assembly Tool,” *Biophys. J.*, vol. 104, p. 169, Jan. 2013.
[90] “Scienomics - Materials and Process Simulations (MAPS),” 2019. [Online]. Available: https://www.scienomics.com/. Accessed on: Mar. 21, 2019.
[91] S. Plimpton, “Fast parallel algorithms for short-range molecular dynamics,” *J. Comput. Phys.*, vol. 117, no. 1, pp. 1–19, 1995.
[92] B. Knapstad, P. A. Skjoelsvik, and H. A. Oeye, “Viscosity of pure hydrocarbons,” *J. Chem. Eng. Data*, vol. 34, no. 1, pp. 37–43, Jan. 1989.
[93] T. Klein *et al.*, “Liquid Viscosity and Surface Tension of n-Hexane, n-Octane, n-Decane, and n-Hexadecane up to 573 K by Surface Light Scattering,” *J. Chem. Eng. Data*, vol. 64, no. 9, pp. 4116–4131, Sep. 2019.
[94] H. G. Yucel and A. Uysal, “Measurements of viscosity and density Of n-alkane and their mixtures,” *Semant. Sch.*, 2005.
[95] D. L. Hogenboom, W. Webb, and J. A. Dixon, “Viscosity of Several Liquid Hydrocarbons as a Function of Temperature, Pressure, and Free Volume,” *J. Chem. Phys.*, vol. 46, no. 7, pp. 2586–2598, Apr. 1967.
[96] D. NguyenHuynh, C. T. Q. Mai, and S. T. K. Tran, “Free-volume theory coupled with modified group-contribution PC-SAFT for predicting the viscosities. I. Non-associated compounds and their mixtures,” *Fluid Phase Equilib.*, vol. 501, Dec. 2019.
[97] P. H. Gross and H. K. Zimmerman, “Properties of the liquid state : II: Description of viscosity over the entire liquid range,” *Rheol. Acta An Int. J. Rheol.*, vol. 3, no. 4, pp. 290–294, 1964.
[98] D. Ambrose and C. Tsonopoulos, “Vapor-Liquid Critical Properties of Elements and Compounds. 2. Normal Alkanes,” *J. Chem. Eng. Data*, vol. 40, no. 3, pp. 531–546, May 1995.
[99] C. Avendaño, T. Lafitte, C. S. Adjiman, A. Galindo, E. A. Müller, and G. Jackson, “SAFT-γ Force Field for the Simulation of Molecular Fluids: 2. Coarse-Grained Models of Greenhouse Gases, Refrigerants, and Long Alkanes,” *J. Phys. Chem. B*, vol. 117, no. 9, pp. 2717–2733, Mar. 2013.
[100] K. A. M. Gasem, C. H. Ross, and R. L. Robinson JR., “Prediction of ethane and CO2 solubilities in heavy normal paraffins using generalized-parameter soave and peng-robinson equations of state,” *Can. J. Chem. Eng.*, vol. 71, no. 5, pp. 805–816, Oct. 1993.
[101] G. Vakili-Nezhaad and H. Sabbaghian-Bidgoli, “Prediction of Critical Properties of Normal Alkanes Using Pakmakar−Ivan Topological Index,” *J.*

Chem. Eng. Data, vol. 56, no. 4, pp. 1042–1046, Apr. 2011.
[102] A. S. Teja, R. J. Lee, D. Rosenthal, and M. Anselme, "Correlation of the critical properties of alkanes and alkanols," *Fluid Phase Equilib.*, vol. 56, no. 1, pp. 153–169, 1990.
[103] C. Tsonopoulos and Z. Tan, "The Critical Constants of Normal Alkanes From Methane to Polyethylene: II. Application of the Flory Theory," *Fluid Phase Equilib.*, vol. 83, pp. 127–138, Feb. 1993.
[104] C. Tsonopoulos, "Critical constants of normal alkanes from methane to polyethylene," *AIChE J.*, vol. 33, no. 12, pp. 2080–2083, Dec. 1987.
[105] K. G. Joback And R. C. Reid, "Estimation Of Pure-Component Properties From Group-Contributions," *Chem. Eng. Commun.*, vol. 57, no. 1–6, pp. 233–243, Jul. 1987.
[106] A. L. Lydersen and E. E. Station, *Estimation of critical properties of organic compounds by the method of group contibutions*. Madison: University of Wisconsin, 1955.
[107] K. M. Klincewicz and R. C. Reid, "Estimation of critical properties with group contribution methods," *AIChE J.*, vol. 30, no. 1, pp. 137–142, Jan. 1984.
[108] R. F. Fedors, "A method to estimate critical volumes," *AIChE J.*, vol. 25, no. 1, p. 202, Jan. 1979.
[109] D. Ambrose, *Correlation and Estimation of Vapour-Liquid Critical Properties : I, Critical Temperatures of Organic Compounds*. London: National Physics Laboratory Division of Chemical Standards, 1978.
[110] D. Ambrose, *Correlation and Estimation of Vapour-Liquid Critical Properties : II, Critical Pressures and Critical Volumes of Organic Compounds*. London: National Physics Laboratory Division of Chemical Standards, 1979.
[111] S. W. I. Siu, K. Pluhackova, and R. A. Böckmann, "Optimization of the OPLS-AA Force Field for Long Hydrocarbons," *J. Chem. Theory Comput.*, vol. 8, no. 4, pp. 1459–1470, Apr. 2012.
[112] J. Ewen, C. Gattinoni, F. Thakkar, N. Morgan, H. Spikes, and D. Dini, "A Comparison of Classical Force-Fields for Molecular Dynamics Simulations of Lubricants," *Materials (Basel).*, vol. 9, no. 8, p. 651, Aug. 2016.
[113] L. H. Eckler and M. J. Nee, "A Simple Molecular Dynamics Lab To Calculate Viscosity as a Function of Temperature," *J. Chem. Educ.*, vol. 93, no. 5, pp. 927–931, May 2016.
[114] M. G. Martin, "Comparison of the AMBER, CHARMM, COMPASS, GROMOS, OPLS, TraPPE and UFF force fields for prediction of vapor–liquid coexistence curves and liquid densities," *Fluid Phase Equilib.*, vol. 248, no. 1, pp. 50–55, 2006.
[115] K. D. Papavasileiou, L. D. Peristeras, A. Bick, and I. G. Economou, "Molecular Dynamics Simulation of Pure n-Alkanes and Their Mixtures at Elevated Temperatures Using Atomistic and Coarse-Grained Force Fields," *J. Phys. Chem. B*, vol. 123, no. 29, pp. 6229–6243, Jul. 2019.

Appendix A

Snapshots of the development of the density profile at different stages of the simulation.

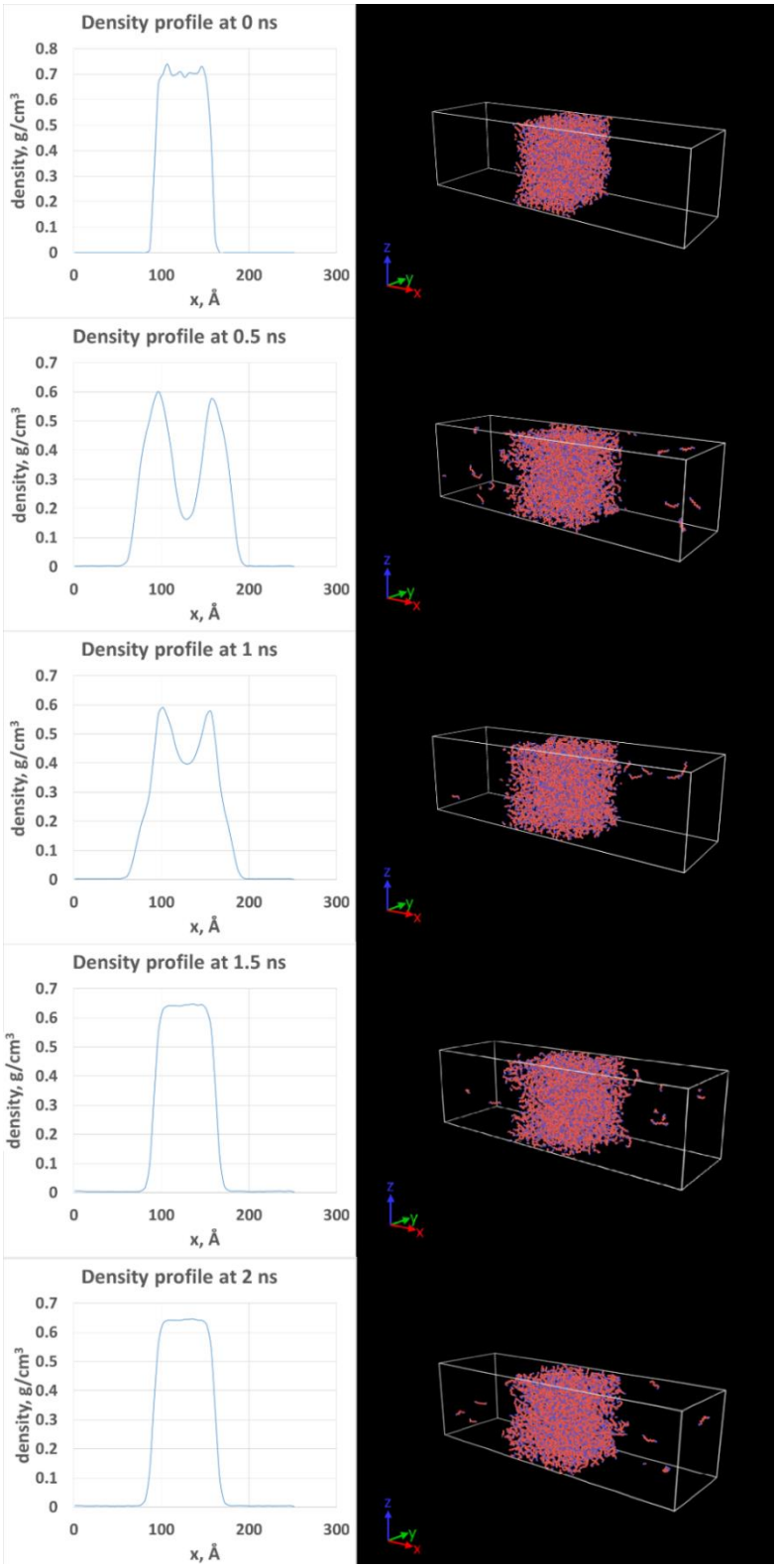

Appendix B

Critical temperatures (T_c) as predicted by different correlations for n-decane, n-pentadecane and n-eicosane.

Table B-1: Prediction of T_c for the three hydrocarbons from different correlations (all values are in K).

Hydrocarbon	Expt. Values	Gasem	Riazi&Sahhaf	Vakili	Teja	Tsonopoulous (1993)
n-decane	617.7	618.2	628.0	620.0	617.9	618.2
n-pentadecane	708.0	707.1	725.0	707.4	707.8	708.1
n-eicosane	768.0	766.6	788.0	766.6	770.9	768.4

Table B-2: Prediction of T_c for the three hydrocarbons from different correlations (all values are in K).

Hydrocarbon	Expt. Values	Tsonopoulous (1987)	Joback	Lydersen	Klincewicz	Ambrose
n-decane	617.7	618.3	617.0	615.2	627.0	617.8
n-pentadecane	708.0	708.0	703.7	700.3	725.0	708.4
n-eicosane	768.0	768.0	766.7	763.6	784.5	770.2

Appendix C

Critical densities (ρ_c) as predicted by different correlations for n-decane, n-pentadecane and n-eicosane.

Table C-1: Prediction of ρ_c for the three hydrocarbons from different correlations (all values are in g/cm^3)

Hydrocarbon	Expt. Values	Riazi&Sahhaf	Vakili	Teja	Tsonopoulous (1993)	Tsonopoulous (1987)
n-decane	0.228	0.255	0.232	0.228	0.228	0.233
n-pentadecane	0.22	0.253	0.222	0.221	0.220	0.234
n-eicosane	0.212	0.251	0.214	0.214	0.214	0.234

Table C-2: Prediction of ρ_c for the three hydrocarbons from different correlations (all values are in g/cm^3)

Hydrocarbon	Expt. Values	Joback	Lydersen	Klincewicz	Ambrose	Fedors
n-decane	0.228	0.239	0.241	0.243	0.241	0.248
n-pentadecane	0.22	0.243	0.246	0.247	0.245	0.254
n-eicosane	0.212	0.245	0.248	0.248	0.247	0.257

Appendix D

Critical pressures (P_c) as predicted by the different correlations for n-decane, n-pentadecane and n-eicosane.

D-1: Prediction of P_c for the three hydrocarbons from different correlations (all values are in MPa)

Hydrocarbon	Expt. Values	Gasem	Riazi&Sahhaf	Vakili	Teja	Tsonopoulous (1993)
n-decane	2.11	2.11	2.42	1.97	2.10	2.10
n-pentadecane	1.48	1.48	1.67	1.49	1.49	1.49
n-eicosane	1.07	1.07	1.14	1.10	1.18	1.17

D-2: Prediction of P_c for the three hydrocarbons from different correlations (all values are in MPa)

Hydrocarbon	Expt. Values	Tsonopoulous (1987)	Joback	Lydersen	Klincewicz	Ambrose
n-decane	2.11	2.10	2.11	2.12	4.98	2.11
n-pentadecane	1.48	1.42	1.42	1.53	3.96	1.53
n-eicosane	1.07	0.996	1.02	1.20	3.26	1.20

Vita

Ibrar Ul Samad was born on 1994, in Dubai. After completing his A-Levels, he joined the BSc Chemical Engineering program at the American University of Sharjah (AUS) in Fall 2013 and graduated Cum Laude in Spring 2017.

In Fall 2017, he joined the MSc. Program in Chemical Engineering at AUS, from where he received a full-time graduate teaching assistantship from Fall 2017 to Spring 2019.